Published in final edited form as:
J Struct Biol. 2011 October ; 176(1): 97–111. doi:10.1016/j.jsb.2011.07.011.

Solution structure and dynamics of ADF from *Toxoplasma gondii*

Rahul Yadav[1], **Prem Prakash Pathak**[1], **Vaibhav Shukla**[1], **Anupam Jain**[1], **Shubhra Srivastava**[1], **Sarita Tripathi**[1], **S.V.S.R. Krishna Pulavarti**[1], **Simren Mehta**[2], **L. David Sibley**[2], and **Ashish Arora**[1,*]

[1]Molecular and Structural Biology Division, Central Drug Research Institute, Lucknow - 226 001, India

[2]Microbiology, Washington University School of Medicine, 660 S. Euclid Ave., St. Louis, Missouri 63110. Tel.: 314-362-8873; Fax: 314-286-0060

Abstract

Toxoplasma gondii (TgADF) belongs to a functional subtype characterized by strong G-actin sequestering activity and low F-actin severing activity. Among the characterized ADF/cofilin proteins, TgADF has the shortest length and is missing a C-terminal helix implicated in F-actin binding. In order to understand its characteristic properties, we have determined the solution structure of TgADF and studied its backbone dynamics from ^{15}N-relaxation measurements. TgADF has conserved ADF/cofilin fold consisting of a central mixed β-sheet comprised of six β-strands that are partially surrounded by three α-helices and a C-terminal helical turn. The high G-actin sequestering activity of TgADF relies on highly structurally and dynamically optimized interactions between G-actin with the G-actin binding surface of TgADF. The equilibrium dissociation constant for TgADF and rabbit muscle G-actin was 23.81 nM, as measured by ITC, which reflects very strong affinity of TgADF and G-actin interactions. The F-actin binding site of TgADF is partially formed, with a shortened F-loop that does not project out of the ellipsoid structure and a C-terminal helical turn in place of the C-terminal helix α4. Yet, it is more rigid than the typical F-actin binding site of *Leishmania donovani* cofilin. Experimental observations and structural features do not support the interaction of PIP2 with TgADF, and PIP2 does not affect the interaction of TgADF with G-actin. Overall, this study suggests that conformational flexibility of G-actin binding sites enhances the affinity of TgADF for G-actin, while conformational rigidity of F-actin binding sites of conventional ADF/cofilins is necessary for stable binding to F-actin.

Keywords

Toxoplasma gondii; TgADF; PIP2; G-actin; NMR; protein dynamics

[*]*Corresponding author*ashishcdri@yahoo.com.
Present address: Molecular and Structural Biology Division, Central Drug Research Institute, Lucknow – 226 001, India. Tel: 91 -522-261 2411-18 ext.4329; Fax: 91-522-262 3405

Introduction

The proteins of the ADF/cofilin family are one of the key regulators of actin filament dynamics and have been shown to be essential for several eukaryotes (Ono, 2007). ADF/cofilin proteins increase the turnover rate of actin filaments by accelerating the dissociation of actin monomers from the filament pointed end. In addition, F-actin filaments are actively severed by several members of the ADF/cofilin family proteins, leading to the generation of new uncapped barbed ends that immediately start growing. The ADF/cofilin proteins manifest their activity through G-actin binding (Lappalainen, et al., 1997), F-actin binding and depolymerization (Lappalainen, et al., 1997), F-actin severing (Andrianantoandro, et al., 2005), controlling the rate of nucleotide exchange from actin monomer (Andrianantoandro, et al., 2005; Hawkins, et al., 1993; Hayden, et al., 1993; Nishida, 1985; Yamashiro, et al., 2005), and actin monomer sequestering activity (Chen, et al., 2004; Mehta and Sibley, 2010; Nachmias, 1993; Yamashiro, et al., 2005). ADF/cofilin proteins show pH sensitivity that is more pronounced in case of the vertebrate than other eukaryote. The F-actin depolymerizing activity (Yonezawa, et al., 1985) of ADF/cofilin proteins is higher at high pH ~8 compared to pH~6.8 (Pope, et al., 2004). However, the activity of ADF/cofilin from *Leishmania donovani* and *Toxoplasma gondii* are pH independent (Mehta and Sibley, 2010; Tammana, et al., 2008).

The non-vertebrate ADF/cofilins represent the highly conserved ADF-homology (ADF-H) fold, which is also observed in destrin, actophorin, and gelsolin. The structure of 143 residues *S. cerevisiae* cofilin consists of a six stranded mixed β-sheet, in which the four central strands are anti-parallel while the two edge strands run parallel to the neighboring strands. The β-sheet is sandwiched between a pair of α-helices on each face. The longest helix (α3) is kinked at the position of a serine residue in a conserved segment. ADF/cofilins have two distinct actin-binding sites. These have been named as the G/F-site and the F-site (Ono, 2003). The G/F-site of ADF/cofilins is required for binding to both the G-actin and the F-actin. This binding site corresponds to helix α3 (long kinked helix), the N-terminal flexible region, the strand β5, and the loop before the C-terminal helix (α4) (Paavilainen, et al., 2008). The F-site is responsible for binding to F-actin and F-actin severing activity. In conventional ADF/cofilins, the F-site is comprised of the β3–β4 loop, also called the 'F-loop', C-terminal helix (helix α4), and the C-terminus. The F-loop typically projects out of the structure and is predicted to intercalate within the actin filament. Sites of ADF/cofilin involved in actin binding have been confirmed by several mutational analysis (Moriyama and Yahara, 1999; Moriyama, et al., 1992; Ono, et al., 1991), cross-linking (Yonezawa, et al., 1991), and peptide competition or synchrotron electron footprinting (Guan, et al., 2002). The G/F-actin binding sites and the F-actin binding sites cluster together in the three-dimensional structure (Fedorov, et al., 1997; Hatanaka, et al., 1996; Pope, et al., 2000) to constitute respective actin binding surfaces.

Vertebrate cofilins are ~160 residues long and in comparison to non-vertebrate subgroup, these have two sequence inserts and an extension of C-terminus. In chick cofilin, human cofilin, and destrin, the first insert is an additional segment bearing helix (α2), in between α1 and β2, which contains a putative nuclear localization sequence (NLS). A second seven residue insert follows β3. In chick cofilin, this insert forms a bulge followed by an additional β-strand that pairs with the N-terminal end of β2 and expands the central β sheet scaffold (Gorbatyuk, et al., 2006). Vertebrate ADF/cofilins also contain a C-terminal extension of approximately eight residues. In chick cofilin, this extension forms a β-hairpin comprising antiparallel strands β7 and β8 that nestle between β4 and α6 (Gorbatyuk, et al., 2006). The sequence of the C-terminal extension may be unique to vertebrate cofilins and it may impart unique F-actin binding properties.

Various activities of ADF/cofilin family proteins have been shown to be dependent on the affinity of these proteins for the actin filaments. It has been observed in the case of the human cofilin that a point mutation of a basic residue K96 in the F-loop leads to a loss of severing activity and increased depolymerizing activity (Pope, et al., 2000). Similarly it has been reported that by mutation, in the F-actin binding sites of ADF/cofilin proteins, severing and depolymerizing activities can be uncoupled (Ono, et al., 1999; Ono, et al., 2001; Pope, et al., 2000). In the case of *Schizosaccharomyces pombe* cofilin, it has been found that the point mutation of R78 in the F-loop resulted in a loss of nucleating activity (Andrianantoandro and Pollard, 2006).

Intracellular protozoan parasites that belong to the phylum Apicomplexa are a significant cause of disease in humans and animals (Joynson and Wreghitt, 2001). Apicomplexa parasites utilize a unique mode of motility, termed gliding, to move across epithelial barriers and translocate into the host cytoplasm (Barragan and Sibley, 2003). Gliding motility is conserved across the Apicomplexa, is dependent on the turnover of actin filaments, and is inhibited by treatment of the parasites with cytochalasin D (Dobrowolski and Sibley, 1996). Although, Apicomplexa actins characterized so far exhibit high sequence homology to the vertebrate actins, they are in contrast typically inherently unstable (Sahoo, et al., 2006; Schmitz, et al., 2005; Schuler, et al., 2005), have significantly lower critical concentration for polymerization (Sahoo, et al., 2006), and yet are almost exclusively unpolymerized in the cytoplasm (Dobrowolski, et al., 1997; Sahoo, et al., 2006, Wetzel, et al., 2003). For example, 98% of actin is present as G-actin in *T. gondii* (Dobrowolski, et al., 1997; Sahoo, et al., 2006, Wetzel, et al., 2003), in comparison to higher eukaryotes where up to 50% cellular actin is in the filament form. Despite the presence of G-actin in high cellular concentration, formation and turnover of filamentous actin is essential for both gliding motility and the host cell invasion by *T. gondii* (Poupel and Tardieux, 1999; Shaw and Tilney, 1999; Wetzel, et al., 2003).

T. gondii expresses a conserved homolog of the ADF/cofilin family (TgADF) that has been shown to play a critical role in actin monomer sequestering and filament disassembly (Mehta and Sibley, 2010). TgADF does not co-sediment with actin filaments. However, it does disassemble actin filaments in pH independent manner but does not form a stable association with actin filaments. TgADF possesses low severing activity, but it inhibits nucleation and polymerization, primarily due to sequestering of actin monomers.

The genomes of Apicomplexa *T. gondii, Eimeria tenella* and *Neospora caninum* express ADF/cofilin proteins that are only 118 residues in length. In these ADF/cofilin proteins, the G/F-actin binding sites are significantly conserved, but there are significant deletions of residues that are required to form the sites for binding F-actin. Specifically, these apicomplexan ADF/cofilins possess a truncated C-terminus and lack the C-terminal charged residues that are predicted as necessary to bind to F-actin. The F-loop is itself much shorter and lacks the conserved basic residue for interaction with F-actin. *Plasmodium* contains two members of the ADF/cofilin family. In *P. falciparum*, the larger of the two, termed as PfADF2, is a 143 residue protein which is closer to the conventional yeast type ADF/cofilin (Schüler, et al., 2005). The shorter ADF, termed as PfADF1, consists of 122 residues, and closely resembles ADF from the other apicomplexans described above. The shorter apicomplexan ADF proteins are the smallest. in the ADF/cofilin family and have not been structurally characterized so far.

In our present study, we have determined the solution structure of TgADF using NMR spectroscopy. Further, we have measured backbone ^{15}N-relaxation rates and have analyzed the dynamics of TgADF in solution using the Lipari-Szabo formalism. We have also determined the thermodynamic parameters characterizing the interaction of TgADF with

rabbit muscle ADP-G-actin using isothermal titration calorimetry (ITC). We also examined the effect of dioctanoyl phosphatidylinositol-4,5-bisphosphate (PIP2), on TgADF itself, and on binding of TgADF to rabbit muscle ADP-G-actin, using ITC and NMR experiments. In order to better understand the structure-function relationship, we have docked the solution structure of TgADF on the crystal structure of G-actin monomer. The docking study has provided us with important insights into the dynamic regulation of structural interaction that lead to high affinity interactions between TgADF and G-actin interactions.

Materials and methods

Preparation of NMR samples

The TgADF protein is composed of 118 amino acid residues with an additional N-terminal twenty-one residue purification tag making the molecular weight of the tagged protein equal to 15480 Da. TgADF was cloned by Mehta and Sibley, (2010). The clone was over-expressed in BL21 (λDE3) strain of *E. coli*. Condition for optimal overexpression and purification were standardized. The yield of purified protein was 30 mg/L of culture medium. For isotopic labeling, over-expressed TgADF was standardized in minimal media containing ^{15}N-ammonium sulfate and ^{13}C-glucose (CIL, MA, USA) as the sole nitrogen and carbon sources, respectively. The additional twenty-one residue purification tag was cleaved by Factor Xa protease at site IEGR according to manufactures guidelines.

NMR samples of ^{13}C / ^{15}N-labeled TgADF were prepared at concentration of approximately 0.8 mM in NMR buffer (20 mM sodium phosphate pH 6.5, 50 mM NaCl, 1 mM DTT, 0.1% NaN_3, and 1 mM AEBSF) containing 95% H_2O / 5% ^2H_2O.

Dioctanoyl-PI(4,5)P2 sample was prepared in G-actin buffer (2.0 mM HEPES, 0.2 mM $CaCl_2$, 0.2 mM ADP, 1.0 mM NaN_3, 1.0 mM BME, pH 7.4) at a concentration of 1 mg/mL (1.34 mM). ^{15}N-labeled TgADF was added to this sample for a final concentration of 0.1 mM for recording the 1D and 2D spectra of TgADF in presence of dioctanoyl-PI(4,5)P2.

NMR spectral assignments

The following experiments were acquired using Varian Biopack package: two-dimensional ^{15}N-^{1}H-HSQC, and three-dimensional HNCACB (Wittekind, et al., 1993), CBCA(CO)NH (Grzesiek, and Bax, 1992), HNCO, HNCA (Kay, et al., 1990), , HN(CA)CO (Clubb, et al., 1992), H(CCO)NH-TOCSY (Montelione, et. al., 1992), (H)C(CO)NH-TOCSY (Grzesiek, et al., 1993), HCCH-TOCSY (Bax, et al., 1990) and ^{15}N-edited NOESY HSQC (τ_{mix} −100 ms), HBHA(CBCACO)NH, 2D-^{13}C-^{1}H-HSQC (aliphatic), ^{13}C-^{1}H-HSQC (aromatic), HB(CBCGCE)HE, and HB(CBCGCD)HD. All spectra were collected at 298 K on Varian Inova 600 MHz spectrometer equipped with actively shielded Z-gradient triple resonance Cold probe. Spectra were processed by using the software NMRPipe (Delaglio, et al., 1995) and analyzed by CARA-1.8.4 (Keller, 2005). The NMR data was referenced for ^{1}H chemical shifts by using 2, 2-dimethyl-2-silapentane-5-sulphonic acid (DSS) at 298 K as a standard. The ^{13}C and ^{15}N chemical shift were referenced indirectly. All NMR experiments were collected at 25 °C. The chemical shifts have been deposited in the BioMagResBank (http://www.bmrb.wisc.edu) under accession number 17278.

Structure calculations

Distance restraints were obtained from 3D ^{15}N-edited NOESY-HSQC spectra (τ_{mix}-150 ms), ^{13}C-edited NOESY-HSQC (τ_{mix}-100 ms and 180 ms), and ^{13}C (aromatic)-edited NOESY-HSQC spectra (τ_{mix}-100 ms). All the spectra were processed using NMRPipe (Delaglio, et al., 1995) and all NOE were assigned manually using CARA-1.8.4 (Keller, 2005). Integrated NOE peaks were calibrated and converted to distance restraints with the

program CALIBA (Guntert, et al., 1991). In the final structural determination, the program CYANA-3.0 (Guntert, et al., 1997) was used. The torsion angle restraints were obtained from assigned backbone chemical shifts using the program TALOS+ (Shen, et al., 2009). A total of 200 randomized conformers were generated and 20 conformers with lowest target function with no distance violation > 0.5 Å and no angle violations were selected. These 20 structures with lowest target function were further subjected to molecular dynamics simulation in explicit water with NMR derived distance restraints and angle restraints using the CNS 1.21 program (Brunger, et al., 1998) and the standard water shell refinement protocol (Jung, et al., 2005; Linge, et al., 2003). At this stage the distances were relaxed and in addition to this $\chi 2$ angles were included for LEU and LYS residues. The $\chi 2$ angles for LEU and LYS residues were kept in the range between 120° and 90°. This step improved the Ramachandran plot statistics and also the Z-score for the Procheck (phi-psi) and Procheck (all) for the ordered residues. The programs CING and PSVS v1.4 (www.psvs-1_4.nesg.org) were used to analyze the quality of the structures. The program PYMOL (http://pymol.sourceforge.net/) was used for generating figures for structures. The charged surface was generated by using program GRASP (Nicholls, et al., 1991).

Relaxation measurements

All relaxation experiments were recorded on uniformly ^{15}N-labeled 0.8 mM N-terminal truncated TgADF sample. The spin-lattice R_1 rate measurements were conducted with relaxation delays of 0, 10, 70, 110, 190, 280, 450, 610, 890, 1100, and 1330 ms. The spin-spin relaxation measurements R_2 were done with Carr-Purcell-Meiboom-Gill delays of 10, 30, 50, 70, 90, 130, 170, 190, and 230 ms. Duplicate ^{1}H-^{15}N HSQC spectra were recorded for every relaxation delay value for both R_1 and R_2 data. The relaxation rates for both R_1 and R_2 were determined from the decay of the intensity of each ^{1}H-^{15}N crosspeaks in this series of spectra. All of the relaxation parameters, along with the { ^{1}H}-^{15}N nuclear Overhauser effect (NOE) intensities for backbone ^{15}N nuclei, were measured at 25 °C, at a magnetic field strength of 14.1 T (corresponding to the resonance frequency of 599.721 MHz for ^{1}H). All the relaxation data were acquired with 96 × 1024 (t1 × t2) complex points and spectral width of 2309.493 Hz and 8401.596 Hz, respectively. The R_1 and R_2 values were obtained by using the program Curvefit. The errors in individual R_1 and R_2 measurements were estimated by Monte Carlo simulations. The steady state heteronuclear {^{1}H}-^{15}N NOE values were obtained by recording spectra with and without proton presaturation period (3 s) applied before the start of the ^{1}H-^{15}N HSQC experiment. The heteronuclear ^{15}N relaxation parameters R_1, R_2, and the steady state heteronuclear {^{1}H}-^{15}N NOE values were analyzed by model-free formalism as described earlier (Clore, et al., 1990; Lipari, and Szabo, 1982a; Lipari, and Szabo, 1982b; Mandel, et al., 1995). For model-free analysis, the N-H bond length was assumed to be 1.02 Å and ^{15}N chemical shift anisotropy value of −160 ppm was considered. The uncertainties in R_1 and R_2 were set to an upper limit of 3% and 5%, respectively. While the uncertainties in steady state heteronuclear {^{1}H}-^{15}N NOE were fixed at 0.05. R_1, R_2, and steady state heteronuclear {^{1}H}-^{15}N NOE were subjected to model-free analysis (Mandel, et al., 1995; Palmer, et al., 1991; Pulavarti, et al., 2008; Roger and Loria, 2003). The dynamic parameters were extracted by using five simple models as proposed by Palmer and coworkers using Modelfree 4.1 program (Palmer et al., 1991). The models considered were : (1) S^2 only, τ_e & R_{ex} are negligible; (2) S^2 and τ_e only, R_{ex} is negligible; (3) model 1 and R_{ex} term; (4) model 2 and R_{ex} term; (5) incorporation of an additional order parameter for anisotropic rotational diffusion.

The ratio of principal components of inertia tensor, calculated using the software Pdbinertia (http://biochemistry.hs.columbia.edu/labs/palmer/software/pdbinertia.html), for the solution structure with lowest target function was found to be 1.0:0.79:0.66, suggesting that the molecule could be diffusing in an axially symmetric manner. Therefore, the fitting of the

residues to different models of Modelfree was done separately with the isotropic diffusion tensor and the axially symmetric diffusion tensor. The calculated D-ratio (D-ratio = 1.18) value indicates small anisotropy which might represent an intermediate state between isotropic and axially symmetric diffusion tensor. However, the relaxation data is well described by an isotropic diffusion tensor. A final optimization of *R1, R2*, and steady state heteronuclear $\{^1H\}$-^{15}N NOE value for the residues that were assigned to any of the five motional models yielded $\tau_m = 6.20 \pm 0.02$ ns.

Isothermal Titration Calorimetry

ITC experiments were performed at 25 °C on a VP-ITC calorimeter from MicroCal™ (Northampton, MA, USA). The calorimeter was calibrated according to the user manual of the instrument. All the samples were briefly centrifuged and then degassed for 20 min before each of the ITC experiments. Titrations were performed at least in duplicate using the same set of stock solutions. The ITC experiments were performed by adding aliquots of ligands to rabbit muscle actin. The rabbit muscle actin for the experiments was prepared as mentioned earlier (Pardee and Spudich, 1982; Pathak, et al., 2010). Stock solution of TgADF and rabbit muscle actin were dialyzed extensively against the HEPES buffer (G-actin buffer) (2.0 mM HEPES, 0.2 mM $CaCl_2$, 0.2 mM ADP, 1.0 mM NaN_3, 1.0 mM BME, pH 7.4). The sample cell was filled with 1.459 mL of 0.003 mM of rabbit muscle actin (titrand) and titrated against TgADF which was filled in the syringe of 290 μL at a concentration of 0.03 mM. The injectant volume was set at 10 μL per injection, and the duration of the injection was 20 s, with an interval of 180 s between injections. During the titration, the reaction mixture was continuously stirred at 351 rpm. Control experiments were performed by injecting TgADF into G-actin buffer under condition exactly similar to the rabbit muscle actin/titrand titration, to take into account heats of dilution and viscous mixing. The heats of injection of the control experiment were subtracted from the raw data of rabbit muscle actin and titrand titration.

Dioctanoyl L-α-Phosphatidyl-D-myo-inositol 4,5-diphosphate (dioctanoyl-PI(4,5)P2) was purchased from Sigma-Aldrich. The stock solutions of dioctanoyl-PI(4,5)P2 were prepared by dissolving 1mg of the lipid either in 1 mL of G-actin buffer without TgADF, or in 1 mL of G-actin buffer having 0.03 mM TgADF. Titration of TgADF-dioctanoyl PI(4,5)P2, and dioctanoyl PI(4,5)P2 to G-actin was done in similar conditions as above for TgADF and G-actin. Control experiments were performed by injecting dioctanoyl-PI(4,5)P2 and TgADF-dioctanoyl-PI(4,5)P2 in buffer.

The ITC data were analyzed using the ORIGIN version 7.0 software provided by MicroCal™. The heats of binding were normalized with respect to the titrand concentration, and a volume correction was performed to take into account dilution of titrand during each injection. The amount of heat produced per injection was calculated by integration of the area under each peak using a baseline selected by the ORIGIN program, assuming a one site binding model. The dissociation constant (*Kd*) and molar enthalpy (ΔH) for the binding of titrand to actin was determined by non-linear least square fitting to the data.

Docking of rabbit muscle actin monomer with TgADF

The Crystal structure of C-terminal ADF-H domain of Twinfilin (Twc) in complex with G-actin monomer (PDB ID: 3DAW) was taken as a template to build a docked model of TgADF with G-actin monomer. TgADF shares only 12% sequence identity with Twc. However, residues in the helix α3 region which is important for the G-actin binding are highly conserved. We used GRAMM-X protein-protein docking web server V-1.2.0 which is publicly available (http://vakser.bioinformatics.ku.edu/resources/gramm/grammx) for docking studies. In order to validate the docking program we analyzed the details of

interface of Twc and G-actin monomer crystal structure (PDB ID: 3DAW) by using the web based server PDBePISA (http://www.ebi.ac.uk/msdsrv/prot_int/pistart.html). Thereafter, we separated the Twc and G-actin monomer from the crystal structure and used the actin and Twc as receptor and ligand, respectively, for docking at the GRAMM-X protein-protein docking server. The details of interface of the Twc docked over G-actin monomer were reanalyzed using the server PDBePISA. Now, TgADF was taken as ligand and the G-actin monomer from the crystal structure of PDB ID 3DAW, after removing the Twc from it, was taken as receptor and docked using the GRAMM-X protein-protein docking server. The details of the interface area were analyzed by using the web based server PDBePISA (http://www.ebi.ac.uk/msdsrv/prot_int/pistart.html).

Result

Assignments and Data deposition

Backbone resonance assignments were made for 107 out of the 113 possible H_N/N crosspeaks in the ^{15}N-^{1}H HSQC spectrum (Fig. 1; 118 residues excluding 5 prolines). The ^{15}N-^{1}H HSQC spectrum of ^{15}N labeled TgADF, with assignments of residues name and number, is shown in Fig. 1. Main chain amide proton assignments were not made for the residues I20, T23, V24, N33, T34 and N67. Assignments for 98.3% of Cα, Cβ and C', and 79.72% of non-aromatic and non-carboxyl side-chain carbons, 62.5% of aromatic side chain carbon, 89.7% of Hα, and 90.2% of Hβ were completed.

Structure determination and statistics

Structural parameters for the solution structure of TgADF are summarized in Table 1. The ensemble of 10 structures, ribbon representation, and electrostatic potential surface for the lowest energy minimized structure is shown in Fig. 2. The pair wise RMSD for the ordered region and the secondary structured region of the ensemble of 10 structures is 0.9 Å and 0.7 Å, respectively. The atomic coordinates for all 10 structures have been deposited in the Protein Data Bank (PDB ID: 2L72).

The solution structure of TgADF can be conventionally related to the canonical ADF/cofilin fold found in the ADF/cofilin, twinfilin, and drebrin/abp1 families of actin binding proteins (ABPs) (Lappalainen, et al., 1998). The core of the TgADF consists of a central six-stranded mixed β-sheet that is encased by helices α1 and α3 on one face and by helix α2 and the C-terminal end of the TgADF, on the opposite face. The strand ordering is β1–β3–β2–β4–β5–β6, in which four central strands are antiparallel and strands β1–β3 and β5–β6 run parallel to each other. The β-strands are β1 (G6–V7), β2 (W26-E32), β3 (K35-G42), β4 (F60-D64), β5 (I69–W74) and β6 (A105–A108), and the α-helices are α1 (E9–L18), α2 (N45-A52), and α3 (V81-L98). Close to the C-terminal of TgADF, there is a short helical turn involving the residues M111-L114. The orientation of this helical turn is fixed due to NOEs observed between residues of this region and residues around the helix α2. The helix α1 is parallel to the strand β2 and helix α3 is parallel to the strand β5. The longest helix α3 in the structure of TgADF is slightly kinked, almost in the center, at residues S89 and S90. This kinking, which is a conserved structural feature of ADF/cofilins, is well supported by observed NOEs between side chain of L94 (helix α3) and F60 (strand β3) and between S90 and L94 of helix α3 and I31 of strand β2. Long range NOEs were observed between residues of helix α3, strand β5, and the loop connecting strand β2–β3. These NOEs define the position of the helix α3. The solution structure of TgADF is stabilized by a few salt bridges in the structure. The C-terminal of the helix α1 is stabilized by the salt bridges clustered between E17 and R21 (C-terminal of α1), K25 (β2), and K43 (β3). The interaction of helix α1 and strand β3 is stabilized by the salt bridge between R14 (α1) and D41 (β3). K19 of helix α1 also forms salt bridge with D99 present at the C-terminal end of the helix α3. Another salt bridge is

present between R59 (β4) and E39 (β3) and D57, which stabilizes the interaction of strand β3 and strand β4. The salt bridges are supported by the presence of NOE cross peaks between the backbone and side chains of the residues forming salt bridges and were visualized in the program Discovery Studio (DS 2.1).

Comparison of TgADF structure with other ADF/cofilin proteins in the Protein Data Bank was carried out using the program DaliLite version 3.0 (Holm, et al., 2008). TgADF has structural similarity with *Acanthamoeba* actophorin (sequence identity 39%, PDB ID: 1CNU) with Z-score of 12.1 and RMSD of 2.6 Å. TgADF shares RMSD of 2.4 Å with plant ADF (sequence identity 47%, PDB ID: 1F7S) and *Schizosaccharomyces pombe* (sequence identity 42%, PDB ID: 2I2Q). However, it shares higher RMSD with vertebrate ADF/cofilin structures. It has RMSD of 2.8 Å, 2.9 Å, and 3.3 Å with Twinfilin C-terminal ADF-H domain (sequence identity 15%, PDB ID: 3DAW), chicken cofilin (sequence identity 34%, PDB ID: 1TVJ), and human non-muscle cofilin (sequence identity 36%, PDB ID: 1Q8G), respectively.

The solution structure of TgADF varies from the other ADF/cofilin structure in terms of the surface charge distribution that is important for dioctanoyl-PI(4,5)P2 interaction. Residues K95, K96, W104, K112, K114, K125, K126, K127, K132, and H133 are conserved in mouse cofilin 1, human cofilin 1, chicken cofilin 1, and human destrin. The cluster of these residues confers a large positively charged surface which is critical for dioctanoyl-PI(4,5)P2 binding. In TgADF, the corresponding residues are C65, G66, W74, K82, R84, L95, K96, K97, T102, and A103, which do not yield a large positively charged surface similar to vertebrate analogs. The charged residues in TgADF are labeled and shown in Fig. 2C. C65 and G66 are present at the F-loop (loop connecting β4–β5). The residues K82–K97 are present on the helix α3, while T102 and A103 are at the N-terminal of strand β6.

Backbone Dynamics of TgADF

To gain an insight into the backbone dynamics of TgADF in solution, we measured ^{15}N longitudinal relaxation rates (R_1), transverse relaxation rates (R_2) and $\{^1H\}$-^{15}N heteronuclear NOEs. The backbone relaxation rates of 85 out of 113 non proline residues were calculated by using the program Curvefit. The average values of relaxation parameters for these residues are $R_1 = 1.78\ s^{-1}$, $R_2 = 8.77\ s^{-1}$, and steady state heteronuclear $\{^1H\}$-^{15}N NOE = 0.76. The residue specific R_1, R_2 and steady state heteronuclear $\{^1H\}$-^{15}N NOE values obtained for TgADF at 600 MHz are shown in Fig. 3. The relaxation parameters were subjected to Modelfree analysis (Mandel, et al., 1995; Palmer, et al., 1991; Pulavarti, et al., 2008; Roger and Loria, 2003), which yielded a rotational correlation time (τ_m) of 6.20± 0.02 ns for the protein molecule. In Modelfree analysis, 84 residues could be fitted while one residue, A2, remained unfitted. The average generalized order parameter S^2 for the 84 fitted residues is 0.88 ± 0.02. 61 residues were fitted to model 1, with an average $S^2 = 0.91 \pm 0.01$; ten residues were described by model 2, with an average $S^2 = 0.79 \pm 0.02$; ten residues were described by model 3, with an average $S^2 = 0.87 \pm 0.01$; one residue was described by model 4 with S^2 value of 0.81± 0.02; two residues were described by model 5, with an average $S^2 = 0.55 \pm 0.01$. Most of the residues fitted in model 1 lie in regions having secondary structure.

The generalized order parameter S^2, the effective correlation time τ_e, and chemical exchange parameter R_{ex} versus residues number is shown in Fig. 4. The generalized order parameter S^2 for N-terminal, F-loop, and C-terminal are 0.45 ±0.02, 0.88 ± 0.01, and 0.82 ± 0.02, respectively, indicating that the N-terminal is far more flexible in comparison to the F-loop and the C-terminal. The residues L18, R21 (C-terminal of α1) K22, N78, K82 (α3), L98 (α3), G100 (loop between α3 and β6), A103, V104 (loop between α3 and β6), E107 (β6), and E110, show R_{ex} term ranging from 1.15 to 5.97 Hz. Residues G4, M5, G6, K35,

I36, D57, R59, K68, S89, D92, E107, H109, L114, show effective correlation time and are expected to undergo fluctuations on fast picoseconds-to-nanosecond time scale. The ribbon representations of lowest energy TgADF structure shaded according to residue specific generalized order parameters (S^2), effective correlation time (τ_e) and conformational exchange term (R_{ex}) are shown in Fig. 5 Essentially similar results were obtained when the relaxation data was analyzed by using the axially symmetric diffusion tensor. The generalized order parameter S^2, the effective correlation time τ_e, and chemical exchange parameter R_{ex} versus residues number for axially symmetric diffusion tensor are shown in Supplementary Fig. 1. The comparison of the residues fitted to different Modelfree models, for the isotropic diffusion tensor and axially symmetric diffusion tensor, is shown in Supplementary Table 1.

Isothermal Titration Calorimetry

The structural features of TgADF are well supported by a direct demonstration of its binding with rabbit muscle G-actin in the presence of ADP. Isothermal titration calorimetry (ITC) titration of TgADF with ADP-G-actin reveals 1:1.23 stoichiometry and a dissociation constant Kd of 23.81 nM, with ΔG of -10.39×10^4 cal/mole, ΔH of $-1.39 \times 10^4 \pm 175.5$ cal/mole and ΔS of −11.80 cal/mole K. The binding of TgADF to G-actin is enthalpy driven. The ITC curve is shown in Fig. 6. The experiments were repeated three times with varying protein concentrations.

The ITC titrations also show that neither ADP-G-actin nor TgADF, in G-actin buffer, interact with dioctanoyl-PI(4,5)P2. The interaction of TgADF with dioctanoyl-PI(4,5)P2 was confirmed by titrating TgADF with dioctanoyl-PI(4,5)P2 (Fig. 7A). The interaction of TgADF with G-actin in the presence of dioctanoyl-PI(4,5)P2 was confirmed by first titrating dioctanoyl-PI(4,5)P2 with G-actin (Fig. 7B), and then the G-actin–dioctanoyl-PI(4,5)P2 mixture with TgADF (Fig.7C). The ITC data shows that the stoichiometry of interaction is 1:1.40 with a dissociation constant Kd of 69.44 nM with ΔG of -9.76×10^4 cal/mole, ΔH of $-1.15 \times 10^4 \pm 409.7$ cal/mole and ΔS of −19.2 cal/mole K, which is compatible with results obtained from titrating TgADF alone with G-actin. A similar S-shaped one-binding site thermogram was obtained, although with higher baseline noise, when a mixture of TgADF-dioctanoyl-PI(4,5)P2 was titrated with G-actin. The lack of structural interaction between TgADF and dioctanoyl-PI(4,5)P2 was also confirmed by recording ^{1}H-^{15}N-HSQC spectra of ^{15}N-labeled -TgADF in the presence and absence of dioctanoyl-PI(4,5)P2. The 1D proton spectra of dioctanoyl-PI(4,5)P2 with and without TgADF is shown in Fig. 7D. In Fig. 7E, the overlapped ^{1}H-^{15}N-HSQC spectra of Tgadf and Tgadf-dioctanoyl-PI(4,5)P2 are shown. No chemical shift perturbation of TgADF peaks is seen in the presence of ~10 fold molar excess of dioctanoyl-PI(4,5)P2.

Docking of rabbit muscle actin monomer with TgADF

We used GRAMM-X protein-protein docking web server V-1.2.0 for generating a docked model of TgADF with rabbit muscle G-actin monomer. The details of interface area of TgADF docked onto G-actin monomer are given in Table 2. In our TgADF-actin docked model, several hydrogen bonds were observed between the residues of TgADF and G-actin. The residue S89 (α3) of TgADF formed hydrogen bonds with residues A144 and Y143 from helix connecting the subdomain 1 and 3 of actin. Residues A93 (α3) and K96 (α3) of TgADF formed hydrogen bonds with residues T351 and M355, respectively, from subdomain 1 of the actin. The strand β6 of TgADF interacted with helix connecting the subdomain 1 and 3 of actin through a hydrogen bond between E107 (β6) of TgADF and R147–T149 of G-actin. N-terminal of TgADF also interacted with subdomain 1 of the actin by forming hydrogen bond between backbone amide of G4 of TgADF and backbone

carboxyl of G23 of actin. The interactions between TgADF and G-actin are depicted in Supplementary Fig. 2.

In our TgADF-actin docked model, residues M1, A2, and S3 from N-terminal were in close proximity to the residues D24, D25, L349, and I345 from subdomain 1 of G-actin. The residues V81, K82, M85, A88, D92, and K97 from helix α3 of TgADF were in close proximity to residues P332, P333, E334, N296, K326, and E167 from subdomain 3 of G-actin. The residues V104 (β6), H109, and E110 of TgADF were in close proximity to the residues S145 and Y143 from helix connecting subdomain 1 and 3 of actin, respectively. The TgADF and G-actin interacting residues in our TgADF-G-actin docked model is further supported by *in-silico* mutational analysis. We generated two models from the lowest energy minimized solution structure of TgADF: 1) K96D; E107K and 2) K82D; R84D. These two models were energy minimized and re-docked as described above in materials and methods. It was found that these two models failed to dock onto G-actin at the cleft between subdomain 1 and 3. The docking study of the mutated models is also supported by previous study where the mutants R96A, K98A and D123A of yeast cofilin (corresponding to K82, R84 and E107 of TgADF) were found to cause defects in interaction with actin (Lappalainen, et al., 1997)

The comparison of TgADF-actin docked model and Twc in complex with the G-actin monomer shows that the residues Y143, A144, R147, T148, and T149 from the helix connecting subdomain 1 and subdomain 3; T351, I345, and E334 of subdomain 1; and E167 from subdomain 3, are common in interaction of TgADF and Twc with G-actin. The buried interface area for the Twc in complex with the G-actin monomer is ~1200 $Å^2$ (15.2%) and for the TgADF-actin docked model it is ~1000 $Å^2$ (16%). The percentage of interacting residues at the interface of the Twc-actin is 21.4% while that for the TgADF-actin interface, it is 23.7%. The helix α3 is the region through which both Twc and TgADF are primarily interacting with the G-actin monomer at the cleft between subdomain 1 and 3. However, the orientation of the helix α3 with respect to the cleft is different for the Twc and TgADF. In the TgADF-actin docked model, complete helical length of helix α3 fits at the cavity formed by subdomain 1 and 3 of actin, while in case of crystal structure of Twc in complex with the G-actin only half of the complete helical length of helix α3 fits in the cavity and rest half of the helix does not participate in interaction with G-actin. This apparent difference in the orientation of the helix α3 of TgADF and Twc at the cavity of subdomain 1 and 3 of actin is clearly noticeable as can be seen from the Supplementary Fig.3.

Discussion

The gliding motility of the apicomplexan parasite *Toxoplasma gondii* is essential for it to invade host cells and to egress from this intracellular niche once replication is complete (Sibley, 2010). Productive gliding motility requires rapid turnover of actin filaments, which is carefully regulated by small subset of actin binding proteins formins, profilins, capping protein, ADF, cyclase-associated protein, and coronin (Carlier, et al., 1997). *T. gondii* actin is relatively unstable and under conditions suitable for formation of F-actin, it only forms small oligomers that sediment at 350,000 × g. Interestingly, 98% of the actin is unpolymerized in *T. gondii*, even though it lacks a dedicated G-actin sequestering protein, such as â-thymosin (Nachmias, 1993). Additionally, TgProfilin, although essential for gliding motility, shows only weak sequestering activity towards heterologous actin (Plattner, et al., 2008). Since TgADF possesses high net F-actin disassembling activity in conjunction with low severing activity, it has been proposed to be a prime candidate for controlling the filament turnover. Genetic knockdown of TgADF confirms this prediction, as in the absence of normal levels, enhanced filamentous actin formation impedes motility and cell invasion (Mehta and Sibley, 2011). The biochemical properties of TgADF have been studied in detail

(Mehta and Sibley, 2010) and it belongs to a specific functional subtype shared with *C. elegans* ADF/cofilin homologue Unc60A (Ono and Benian, 1998), and embryonic chick skeletal muscle ADF (Abe and Obinata, 1989). This functional subtype is characterized as having the following activities: an inhibitory effect on actin polymerization; strong sequestration of monomeric actin (G-actin); inhibition of actin nucleation; inhibition of nucleotide exchange by G-actin; weak F-actin severing activity; lack of stable F-actin binding; and highly efficient net disassembly of F-actin. Moreover, the TgADF activity is independent of pH. The high monomer sequestering activity and low severing activity has been associated with the scenario where the actin filaments must be rapidly assembled and disassembled (Mehta and Sibley 2010).

From a primary sequence viewpoint, TgADF belongs to a specific subgroup of ADF/cofilin family having the smallest number of residues within the ADF/cofilin family. TgADF has high sequence homology (75%) to the shorter *Plasmodium* ADFs. With respect to TgADF, the shorter *Plasmodium* ADFs have a one residue insert after the C-terminus residue G42 of strand β3, and a three residues insert after the residue D57 in the loop connecting α2 to β4. The position of these residues is such that it does not affect interaction with actin. Therefore, the biochemical properties and structural properties of shorter ADFs of *Plasmodium* are expected to be very similar to that of TgADF.

The solution structure of TgADF is characterized by conserved ADF/cofilin fold with the N-terminal flexible region, conserved long kinked helix, shortened F-loop that did not project beyond the overall ellipsoid structure, and a truncated C-terminal having a short helical segment in place of the helix α4. The G-actin binding site of the TgADF is well formed and is defined by the long kinked helix α3, the N-terminal flexible region, the strand β6, and loop before the C-terminal helical turn (Paavilainen, et al., 2008). The ^{15}N-relaxation dynamics of residues in this region also have desired flexibility to facilitate the interaction of TgADF with G-actin monomer. The docking of TgADF with rabbit muscle G-actin monomer suggests that the complete helical length of helix α3 of TgADF interacts with G-actin. The helix α3 in the TgADF has positively charged residues K82 at its N-terminus, while it has two contiguous charged residues, K96 and K97, at its C-terminus. The latter feature is also observed in human ADF (Yeoh, et al., 2002) and actophorin (Blanchoin, et al., 2000). Infact, residue K125 of human ADF, which corresponds to K96 of TgADF, has been shown to interact with actin. The residues V81, K82, M85, A88, D92, A93, K96, and K97 from helix α3 of TgADF were found to interact with the G-actin. The two residues S89 and D92 at the center of helix α3 are flexible as indicated by effective correlation time. Moreover, the residues at both the ends of the helix α3 (K82 and L98) show conformational exchange. The G-actin interacting residues of TgADF involved in hydrogen bonding as shown in Fig. 8B are on the same face with the residues showing conformational exchange and effective correlation time (Fig. 8A). In addition to the helix α3, other interacting residues are from the N-terminal region, strand β6, and the segment preceding C-terminal helical turn. Interestingly, many of these residues, for example, N78, G100, A103, V104 (β6), E107 (β6), are similarly involved in conformational exchange on milli-to-microsecond time scale. Thus, overall it seems that TgADF is structurally and dynamically suited to have highly optimized interactions with G-actin.

The dynamically optimized interaction of TgADF with G-actin is reflected in the equilibrium dissociation constant of 0.02 μM measured with the ITC experiments, ITC experiments were done with rabbit muscle ADP-G-actin. For a direct comparison of ITC results, the equilibrium dissociation constant for the interaction of ADF/cofilin protein from *Leishmania donovani* with ADP-G-actin, also obtained from ITC experiments (Pathak, et al., 2010), has been reported to be ~0.2 μM. High affinity in similar range (2–30 nm *Kd*) has been observed between Mouse ADF/cofilins (cofilin-1, cofilin-2, or ADF) and Mg-ADP-G-

actin through fluorometric measurements using NBD-labeled actin samples (Vartiainen et al., 2002). Given that the binding affinity determined with flurometric methods is slightly higher than that determined by ITC, we believe that the interaction between TgADF and G-actin, and that of mouse ADF/cofilin with G-actin, may very well reflect the strongest possible interactions for this pair of proteins, as most of the other ADF/cofilin proteins bind to ADP-G-actin with affinities of 0.5–1 μM. The structural features of TgADF have to be examined in view of this high affinity for ADP-G-actin. Usually there is a 10 to 20-fold decrease in the affinity for Mg-ATP-G-actin in comparison to ADP-G-actin. Previously, the apparent affinity of 0.64 μM has been reported between TgADF and Mg-ATP-G-actin, which was determined on the basis of the effect of TgADF on the rate of nucleotide exchange by G-actin (Mehta and Sibley, 2010). The affinity of TgADF for Mg-ATP-G-actin is in the same range as other members of its functional subtype. For example, Unc60A and chick ADF have affinities for Mg-ATP-G-actin of ~1.6 μM and 1 μM, respectively (Chen, et al, 2004; Yamashiro, et al, 2005). The large difference between the affinities of TgADF for ADP-G-actin versus ATP-G-actin may provide thermodynamically the driving force needed for highly efficient disassembly of F-actin.

In conventional ADF/cofilins, the F-loop includes a pair of basic residues at the beginning of the β5 strand. The C-terminal α4 helix, and/or the C-terminal tail, also contain some charged residues. These F-loop basic residues and C-terminal charged residues together can increase the stability of interaction of ADF/cofilin for F-actin, leading to increased severing activity (Lappalainen, et al., 1997; Ono, et al., 2001; Pope, et al., 2000). It has been observed for many systems that the net filament disassembly activity is inversely related to stability of interaction with F-actin. Pope *et. al.*, (2004) have demonstrated that mutating the first (R96 in *S. pombe* cofilin, K68 in TgADF) of the two basic residues in the F-loop region that are critical for F-actin binding, results in human cofilin losing its ability to bind F-actin, and instead causes it to effect the extensive depolymerization of filaments. It has been shown that introduction of point mutations G66R and G66K in TgADF had little effect on its co-sedimentation or disassembly of actin filaments (Mehta and Sibley, 2010), suggesting that the position and orientation of nearby basic residue K68 might be more important for F-actin severing activity. On the other hand, extension of C-terminal of TgADF with a seven residue charged segment, corresponding to the last seven residues of *S. pombe* cofilin, resulted in a 2-fold increase in the amount of TgADF co-sedimenting with F-actin and decreased disassembly of F-actin (Mehta and Sibley, 2010).

In the TgADF solution structure, the F-loop comprises the β - β turn connecting strand β4 and strand β5 and contains a total of 15 residues (β4: 5 residues; β5: 6 residues; interconnecting loop: 4 residues). Unlike all the other ADF/cofilin proteins, this segment does not project out of the structure because of its short length. In the solution structure of TgADF, the C-terminal helix α4 is not properly formed and in its place there is a three residue helical turn. Yet, in terms of dynamics, both the F-loop, and the C-terminal regions are fairly rigid, except for residues N67 and K68 that are at the tip of F-loop. This allows for an interesting comparison with the solution structure of LdCof. In LdCof, the F-loop contains a total of 23 residues (β4: 10 residues; β5: 11 residues; interconnecting loop: 2 residues), i.e. 8 residues more than TgADF, and the F-loop duly projects out of the structure. The turn residues connecting β4 and β5 are K77 and R78, i.e. basic residues. The C-terminal of LdCof has a properly formed helix α4 and also several basic residues are present in the C-terminal tail. The average S^2 value of N-terminal, F-loop and C-terminal for TgADF are 0.45, 0.88 and 0.82, respectively, while the corresponding values for LdCof are 0.43, 0.76 and 0.35, respectively. This shows that while the N-terminal segments of TgADF and LdCof are equally flexible, the F-loop and C-terminal segment of TgADF are rigid in comparison to the corresponding regions of LdCof (Fig. 8C, 8D). Although, LdCof conforms to all of the above described features for stable interaction with F-actin, yet it has been

experimentally demonstrated that it does not co-sediment with rabbit muscle F-actin, and it has weak F-actin severing activity. Our current understanding is that for stable interaction of ADF/cofilins with F-actin, structural features like an outwardly projecting F-loop and well formed C-terminal helix α4, and biochemical features like presence of basic residues on the F-loop and at the C-terminal of the protein, are essential. Our results highlight the importance of conformational rigidity of the involved structural segments as another feature that may be necessary for stable interactions with F-actin, while for weak F-actin severing activity the presence of a single surface exposed basic residue K68 in TgADF and K80 in LdCof on the F-loop may be sufficient.

The N terminus of ADF/cofilin proteins is highly conserved and in particular the serine 3 residue is an important contact site for interactions with actin. The activity of some AC proteins is negatively regulated by phosphorylation at this site (Allwood, et al., 2002; Gungabissoon, et al., 1998; Ojala, et al., 2001; Yonezawa, et al., 1990). In the case of TgADF, the S3E mutation, which potentially mimics the phosphorylation at this site, made the resulting mutant completely inactive (Mehta and Sibley, 2010). The N-terminal of TgADF is clearly very mobile and structurally poorly defined. However, we could clearly notice a chemical shift perturbation effect for residues I31 (β2) and L94 (α3) upon cleavage of N-terminal purification tag. Therefore, it is imperative that the N-terminal is nestled along the border of helix α3 and strands β2. Incidentally, in TgADF structure S3 is proximal to T34. The residues N33 and T34 located between the loop connecting the strand β2 and β3 could not be assigned due to line broadening and are said to have motion on intermediate NMR timescale. Moreover, contiguous residues K35 and I36 display fluctuations on picoseconds-to-nanosecond time scale. Overall, this gives a picture of highly dynamic N-terminal with residues around S3, especially N33 and T34 from the loop joining β2 and β3, displaying conformational flexibility, perhaps, to accommodate the steric requirements of phosphorylation, although this modification has not been demonstrated in apicomplexans.

The segment R21-K25 of TgADF sequentially overlaps with vertebrate ADF/cofilins viz. destrin, human cofilin-1 and chicken cofilin-2 (Gorbatyuk, et al., 2006; Hatanaka, et al., 1996; Pope, et al., 2004), where this region corresponds to an insert that contains a putative nuclear localization signal (NLS) which is believed to be responsible for the nuclear translocation of ADF/cofilin proteins upon cellular stresses. It has been proposed that this region may be undergoing an exchange between a helical and extended conformation, and may, therefore, function as a molecular switch to dictate the cellular localization of vertebrate ADF/cofilin proteins. The putative NLS sequence in vertebrates is also believed to be responsible for the formation of nuclear cofilin:actin rods (Nishida, et al., 1987). The residues L18, R21 and K22 from the segment R21-K25 display conformational exchange on millisecond-to-microsecond time scale. These residues are near to the residues I20, T23, and V24 located between the helix α1 and strand β2 which could not be assigned due to line broadening. These missing residues in ^{15}N-HSQC are expected to undergo intermediate motion on the NMR timescale making them intractable in backbone assignment experiments. This suggests that the segment L18-K25 is most likely undergoing conformational exchange between two stable conformers and could have some undiscovered role in interaction with other proteins. The structure and dynamics of segment R21-K25 of TgADF are shown in Fig 9A, and for comparison the corresponding NLS region of human cofilin-1 is highlighted in Fig. 9B.

TgADF does not show any detectable interaction with dioctanoyl PI(4,5)P2 in ITC and NMR experiments. Moreover, the presence of dioctanoyl PI(4,5)P2 does not interfere with binding of TgADF with rabbit muscle ADP-G-actin. It has been suggested that PIP2 inhibits the ADF/cofilin-actin interaction by steric occlusion of actin binding site on ADF/cofilin (Kusano, et al., 1999; Ojala, et al., 2001; Yonezawa, et al., 1991). Gorbatyuk et al., (2006)

have shown that dioctanoyl-PI(4,5)P2 interacts specifically to the putative F-actin and G-actin binding site on the ADF/cofilin (Gorbatyuk, et al., 2006), but a recent study suggest that this interaction is unspecific and multivalent in nature (Zhao, et al., 2010). The negatively charged phosphate head of dioctanoyl-PI(4,5)P2 interacts with the positively charged surface of the ADF/cofilin (Zhao, et al., 2010). It has been observed that in mouse cofilin-1, human cofilin-1, chicken cofilin-1, and human destrin the positively charged surface is created by the cluster of highly conserved residues K95, K96, W104, K112, K114, K125, K126, K127, K132, and H133 (Fig. 9D). Thus the interaction of dioctanoyl-PI(4,5)P2 with ADF/cofilin needs a cluster of large solvent exposed positively charged amino acid residues on the surface of the ADF/cofilin proteins. The sequence alignment of TgADF with above mentioned cofilin sequences suggests that the positively charged surface in TgADF is contributed by a much smaller cluster of positively charged residues K82, R84, K96, and K97 all from helix α3 (Fig. 9C), and therefore lacks the large patch required for interacting with the negatively charged head of dioctanoyl-PI(4,5)P2.

In conclusion, we have presented the first solution structure of an apicomplexan ADF protein and have characterized its complete backbone dynamics, its affinity for G-actin in the presence of ADP, and its binding to dioctanoyl-PIP2. The novelty of work is in recognizing the high affinity of TgADF for ADP-G-actin and its lack of interaction with PIP2. Moreover, based on the comparison of dynamics of TgADF with LdCof and other ADF/cofilin proteins, we can conclude that conformational rigidity of F-actin binding sites of ADF/cofilin is necessary for stable binding to F-actin, while for weak F-actin severing activity the presence of a single surface exposed basic residue K68 in TgADF and K80 in LdCof on the F-loop may be sufficient.

Supplementary Material

Refer to Web version on PubMed Central for supplementary material.

Acknowledgments

This work was supported by grants from CSIR Network NWP0038. R.Y. is recipient of research fellowships from DBT, India. P.P.P., and V.K.S are recipient of research fellowships from the Council of Scientific and Industrial Research (CSIR), New Delhi, India. S.S. is recipient of research fellowships from ICMR, India. We thank Prof. C.L. Khetrapal, Director, CBMR, Lucknow, for access to the Bruker 800 MHz spectrometer. We thank Dr. Raja Roy, and Dr. Dinesh kumar for help. We thank Dr. Chhitar Mal Gupta, distinguished scientist DBT, India, Dr. Amogh Anant Sahasrabuddhe and Mr. Rajendra Kumar Srivastava for their help in preparing actin.

Reference

1. Abe H, Obinata T. An actin-depolymerizing protein in embryonic chicken skeletal muscle: purification and characterization. J. Biochem. 1989; 106:172–180. [PubMed: 2777748]
2. Allwood EG, Anthony RG, Smertenko AP, Reichelt S, Drobak BK, et al. Regulation of the pollen-specific actin-depolymerising factor, LlADF1. Plant Cell. 2002; 14:2915–2927. [PubMed: 12417710]
3. Andrianantoandro E, Pollard TD. Mechanism of actin filament turnover by severing and nucleation at different concentrations of ADF/cofilin. Mol. Cell. 2006; 24:13–23. [PubMed: 17018289]
4. Barragan A, Sibley LD. Migration of *Toxoplasma gondii* across biological barriers. Trends Microbiol. 2003; 11:426–430. [PubMed: 13678858]
5. Bax A, Clore GM, Gronenborn AM. ^{1}H---^{1}H correlation via isotropic mixing of ^{13}C magnetization, a new three-dimensional approach for assigning ^{1}H and ^{13}C spectra of ^{13}C-enriched proteins. J. Magn. Reson. 1990; 88:425–431.
6. Blanchoin L, Robinson RC, Choe S, Pollard TD. Phosphorylation of *Acanthamoeba* actophorin (ADF/cofilin) blocks interaction with actin without a change in atomic structure. J. Mol. Biol. 2000; 295:203–211. [PubMed: 10623520]

7. Brunger AT, Adams PD, Clore GM, Delano WL, Gros P, et al. Crystallography & NMR system: a new software suite for macromolecular structure determination. Acta Crystallogr. 1998; 54:905–921.
8. Carlier MF, Laurent V, Santolini J, Melki R, Didry D, et al. Actin depolymerizing factor (ADF/cofilin) enhances the rate of filament turnover:implication in actin-based motility. J. Cell Biol. 1997; 136:1307–1323. [PubMed: 9087445]
9. Chen H, Bernstein BW, Sneider JM, Boyle JA, Minamide LS, et al. In vitro activity differences between proteins of the ADF/cofilin family define two distinct subgroups. Biochemistry. 2004; 43:7127–7142. [PubMed: 15170350]
10. Clore GM, Szabo A, Bax A, Kay LE, Driscoll PC, et al. Deviations from the simple two parameter model free approach to the interpretation of ^{15}N nuclear magnetic relaxation of proteins. J. Am. Chem. Soc. 1990; 112:4989–4991.
11. Clubb RT, Thanabala V, Wagner G. A constant-time three-dimensional triple-resonance pulse scheme to correlate intraresidue 1HN, 15N, and 13C′ chemical shifts in 15N---13C-labelled proteins. J. Magn. Reson. 1992; 97:213–217.
12. Delaglio F, Grzesiek S, Vuister GW, Zhu G, Pfeifer J, et al. *NM*RPipe: a multidimensional spectral processing system based on UNIX pipes. J. Biomol. NMR. 1995; 6:277–293. [PubMed: 8520220]
13. Dobrowolski JM, Niesman IR, Sibley LD. Actin in the parasite *Toxoplasma gondii* is encoded by a single copy gene, ACT1 and exists primarily in a globular form Cell Motil. Cytoskeleton. 1997; 37:253–262.
14. Dobrowolski JM, Sibley LD. *Toxoplasma* invasion of mammalian cells is powered by the actin cytoskeleton of the parasite. Cell. 1996; 84:933–939. [PubMed: 8601316]
15. Fedorov AA, Lappalainen P, Fedorov EV, Drubin DG, Almo SC. Structure determination of yeast cofilin. Nat. Struct. Biol. 1997; 4:366–369. [PubMed: 9145106]
16. Gorbatyuk VY, Nosworthy NJ, Robson SA, Bains NP, Maciejewski MW, et al. Mapping the phosphoinositide-binding site on chick cofilin explains how PIP2 regulates the cofilin-actin interaction. Mol. Cell. 2006; 24:511–522. [PubMed: 17114056]
17. Grzesiek S, Bax A. Correlating backbone amide and side chain resonances in larger proteins by multiple relayed triple resonance NMR. J. Am. Chem. Soc. 1992; 114:6291–6293.
18. Grzesiek S, Anglister J, Bax A. Correlation of Backbone Amide and Aliphatic Side-Chain Resonances in ^{13}C/^{15}N-enriched Proteins by Isotopic Mixing of ^{13}C Magnetization. J. Magn. Reson. Series B. 1993; B101:114–119.
19. Guan JQ, Vorobiev S, Almo SC, Chance MR. Mapping the G-actin binding surface of cofilin using synchrotron protein footprinting. Biochemistry. 2002; 41:5765–5775. [PubMed: 11980480]
20. Gungabissoon RA, Jiang CJ, Drobak BK, Maciver SK, Hussey PJ. Interaction of maize actin-depolymerising factor with actin and phosphoinositides and its inhibition of plant phospholipase C. Plant J. 1998; 16:689–696.
21. Guntert P, Mumenthaler C, Wuthrich K. Torsion angle dynamics for NMR structure calculation with the new program DYANA. J. Mol. Biol. 1997; 271:283–298. [PubMed: 9367762]
22. Guntert P, Qian YQ, Otting G, Muller M, Gehring W, Wuthrich K. Structure determination of the Antp (C39----S) homeodomain from nuclear magnetic resonance data in solution using a novel strategy for the structure calculation with the programs DIANA, CALIBA, HABAS and GLOMSA. J. Mol. Biol. 1991; 217:531–540. [PubMed: 1671604]
23. Hatanaka H, Ogura K, Moriyama K, Ichikawa S, Yahara I, et al. Tertiary structure of destrin and structural similarity between two actin-regulating protein families. Cell. 1996; 85:1047–1055. [PubMed: 8674111]
24. Hawkins M, Pope B, Maciver SK, Weeds AG. Human actin depolymerizing factor mediates a pH sensitive destruction of actin filaments. Biochemistry. 1993; 32:9985–9993. [PubMed: 8399167]
25. Hayden SM, Miller PS, Brauweiler A, Bamburg JR. Analysis of the interactions of actin depolymerizing factor with G-and F-actin. Biochemistry. 1993; 32:9994–10004. [PubMed: 8399168]
26. Holm L, Kaariainen S, Rosenstrom P, Schenkel A. Searching protein structure databases with DaliLite v.3. Bioinformatics. 2008; 24:2780–2781. [PubMed: 18818215]

27. Joynson, DH.; Wreghitt, TJ. Toxoplasmosis: A Comprehensive Clinical Guide. New York: Cambridge University Press; 2001.
28. Jung JW, Yee A, Wu B, Arrowsmith CH, Lee W. Solution structure of YKR049C, a putative redox protein from *Saccharomyces cerevisiae* . J. Biochem. Mol. Biol. 2005; 38:550–554. [PubMed: 16202234]
29. Kay LE, Ikura M, Tschudin R, Bax A. Three-dimensional triple-resonance NMR spectroscopy of isotopically enriched proteins. J. Magn. Reson. 1990; 89:496–514.
30. Keller, R. Diss. ETH No. 15947. Swiss federal Institute of Technology; Zurich: 2005. Optimizing the process of nuclear magnetic resonance spectrum analysis and computer aided resonance assignment.
31. Kusano K, Abe H, Obinata T. Detection of a sequence involved in actin-binding and phosphoinositide-binding in the N-terminal side of cofilin. Mol. Cell. Biochem. 1999; 190:133–141. [PubMed: 10098980]
32. Lappalainen P, Fedorov EV, Fedorov AA, Almo SC, Drubin DG. Essential functions and actin-binding surfaces of yeast cofilin revealed by systematic mutagenesis. EMBO J. 1997; 16:5520–5530. [PubMed: 9312011]
33. Lappalainen P, Kessels MM, Cope MJ, Drubin DG. The ADF homology (ADF-H) domain: a highly exploited actin-binding module. Mol. Biol. Cell. 1998; 9:1951–1959. [PubMed: 9693358]
34. Linge JP, Williams MA, Spronk AEM, Bonvin AM, Nilges M. Refinement of protein structures in explicit solvent. Proteins. 2003; 50:496–506. [PubMed: 12557191]
35. Lipari G, Szabo A. Modelfree approach to the interpretation of nuclear magnetic-resonance relaxation in macromolecules I. Theory and range of validity. J. Am. Chem. Soc. 1982a; 104:4546–4559.
36. Lipari G, Szabo A. Modelfree approach to the interpretation of nuclear magnetic resonance relaxation in macromolecules II. Analysis of experimental results. J. Am. Chem. Soc. 1982b; 104:4559–4570.
37. Mandel AM, Akke M, Palmer AG. Backbone dynamics *of Escherichiacoli* ribonuclease HI: correlations with structure and function in an active enzyme. J. Mol. Biol. 1995; 246:144–163. [PubMed: 7531772]
38. Mehta S, Sibley LD. *Toxoplasma gondii* actin depolymerizing factor acts primarily to sequester G-actin. J. Biol. Chem. 2010; 285:6835–6847. [PubMed: 20042603]
39. Mehta S, Sibley LD. Actin depolymerizing factor controls actin turnover and gliding motility in *Toxoplasma gondii* . Mol. Biol. Cell. 2011; 22:1290–1299. [PubMed: 21346192]
40. Montelione T, Lyons BA, Emerson SD, Tashiro M. An efficient triple resonance experiment using carbon-13 isotropic mixing for determining sequence-specific resonance assignments of isotopically-enriched proteins. J. Am. Chem. So. 1992; 114:10974–10975.
41. Moriyama K, Yahara I. Two activities of cofilin, severing and accelerating directional depolymerization of actin filaments, are affected differentially by mutations around the actin-binding helix. EMBO J. 1999; 18:6752–6761. [PubMed: 10581248]
42. Moriyama K, Yonezawa N, Sakai H, Yahara I, Nishida E. Mutational analysis of an actin-binding site of cofilin and characterization of chimeric proteins between cofilin and destrin. J. Biol. Chem. 1992; 267:7240–7244. [PubMed: 1313794]
43. Nachmias VT. Small actin-binding proteins: the beta-thymosin family. Curr. Opin. Cell Biol. 1993; 5:56–62. [PubMed: 8448031]
44. Nicholls A, Sharp KA, Honig B. Protein folding and association: insights from the interfacial and thermodynamic properties of hydrocarbons. Proteins. Struct. Funct. Genet. 1991; 11:281–285. [PubMed: 1758883]
45. Nishida E. Opposite effects of cofilin and profilin from porcine brain on rate of exchange of actin-bound adenosine 5'-triphosphate. Biochemistry. 1985; 24:1160–1164. [PubMed: 4096896]
46. Nishida E, Iida K, Yonezawa N, Koyasu S, Yahara I, et al. Cofilin is a component of intranuclear and cytoplasmic actin rods induced in cultured cells. Proc. Natl. Acad. Sci. USA. 1987; 84:5262–5266. [PubMed: 3474653]
47. Ojala PJ, Paavilainen V, Lappalainen P. Identification of yeast cofilin residues specific for actin monomer and PIP2-binding. Biochemistry. 2001; 40:15562–15569. [PubMed: 11747431]

48. Ono S. Regulation of actin filament dynamics by actin depolymerizing factor/cofilin and actin-interacting protein 1: new blades for twisted filaments. Biochemistry. 2003; 42:13363–13370. [PubMed: 14621980]
49. Ono S. The mechanism of depolymerization and severing of actin filaments and its significance in cytoskeletal dynamics. Int. Rev. Cytol. 2007; 258:1–82. [PubMed: 17338919]
50. Ono S, Baillie DL, Benian GM. UNC-60B, an ADF/cofilin family protein, is required for proper assembly of actin into myofibrils in *Caenorhabditis elegans* body wall muscle. J. Cell Biol. 1999; 145:491–502. [PubMed: 10225951]
51. Ono S, Benian GM. Two *Caenorhabditis elegans* actin depolymerizing factor/cofilin proteins, encoded by the unc-60 gene, differentially regulate actin filament dynamics. J. Biol. Chem. 1998; 273:3778–3783. [PubMed: 9452511]
52. Ono S, McGough A, Pope BJ, Tolbert VT, Bui A, et al. The C-terminal tail of UNC-60B (ADF/cofilin) is critical for maintaining its stable association with F-actin and is implicated in the second actin-binding site. J. Biol. Chem. 2001; 276:5952–5958. [PubMed: 11050090]
53. Paavilainen VO, Oksanen E, Goldman A, Lappalainen P. Structure of the actin-depolymerizing factor homology domain in complex with actin. J. Cell. Biol. 2008; 182:51–59. [PubMed: 18625842]
54. Palmer AG, Rance M, Wright PE. Intramolecular motions of a zinc finger DNA-binding domain from Xfin characterized by proton-detected natural abundance ^{13C} heteronuclear NMR spectroscopy. J. Am. Chem. Soc. 1991; 113:4371–4380.
55. Pardee JD, Spudich JA. Purification of muscle actin. Methods Enzymol. 1982; 85:164–181. [PubMed: 7121269]
56. Pathak PP, Pulavarti SVSRK, Jain A, Sahasrabuddhe AA, Gupta CM, et al. Solution structure and dynamics of ADF/cofilin from *Leishmania donovani* . J. Struc. Biol. 2010; 172:219–224.
57. Plattner F, Yarovinsky F, Romero S, Didry D, Carlier MF, et al. *Toxoplasma* profilin is essential for host cell invasion and TLR11-dependent induction of an interleukin-12 response. Cell Host Microbe. 2008; 3:77–87. [PubMed: 18312842]
58. Pope BJ, Gonsior SM, Yeoh S, McGough A, Weeds AG. Uncoupling actin filament fragmentation by cofilin from increased subunit turnover. J. Mol. Biol. 2000; 298:649–661. [PubMed: 10788327]
59. Pope BJ, Ziegler-Gould KM, Kuhne R, Weeds AG, Ball LJ. Solution structure of human cofilin: actin binding, pH sensitivity, and relationship to actin-deploymerizing factor. J. Biol. Chem. 2004; 279:4840–4848. [PubMed: 14627701]
60. Poupel O, Tardieux I. *Toxoplasma gondii* motility and host cell invasiveness are drastically impaired by jasplakinolide, a cyclic peptide stabilizing F-actin. Microbes Infect. 1999; 1:653–662. [PubMed: 10611742]
61. Pulavarti SVSRK, Jain A, Pathak PP, Mahmood A, Arora A. Solution structure and dynamics of peptidyl-tRNA hydrolase from *Mycobacterium tuberculosis* H37Rv. J. Mol. Biol. 2008; 378:165–177. [PubMed: 18342886]
62. Roger C, Loria JP. FAST-Modelfree: a program for rapid automated analysis of solution NMR spin-relaxation data. J. Biomol. NMR. 2003; 26:203–213. [PubMed: 12766418]
63. Sahoo N, Beatty W, Heuser J, Sept D, Sibley LD. Unusual kinetic and structural properties control rapid assembly and turnover of actin in the parasite *Toxoplasma gondii* . Mol. Biol. Cell. 2006; 17:895–906. [PubMed: 16319175]
64. Schmitz S, Grainger M, Howell S, Calder LJ, Gaeb M, et al. Malaria parasite actin filaments are very short. J. Mol. Biol. 2005; 349:113–125. [PubMed: 15876372]
65. Schüler H, Mueller AK, Matuschewski K. A *Plasmodium* actin depolymerizing factor that binds exclusively to actin monomers. Mol. Biol. Cell. 2005; 16:4013–4023. [PubMed: 15975905]
66. Schuler H, Mueller AK, Matuschewski K. Unusual properties of *Plasmodium falciparum* actin: new insights into microfilament dynamics of apicomplexan parasites. FEBS Lett. 2005; 579:655–660. [PubMed: 15670824]
67. Shaw MK, Tilney LG. Induction of an acrosomal process in *Toxoplasma gondii:* Visualization of actin filaments in a protozoan parasite. Proc. Natl. Acad. Sci. U.S.A. 1999; 96:9095–9099. [PubMed: 10430901]

68. Shen Y, Delaglio F, Cornilescu G, Bax A. TALOS+: a hybrid method for predicting protein backbone torsion angles from NMR chemical shifts. J. Biomol. NMR. 2009; 44:213–223. [PubMed: 19548092]
69. Sibley LD. How apicomplexan parasites move in and out of cells. Curr Opin Biotechnol. 2010; 5:592–598. [PubMed: 20580218]
70. Tammana TVS, Sahasrabuddhe AA, Mitra K, Bajpai VK, Gupta CM. Actin-depolymerizing factor, ADF/cofilin, is essentially required in assembly of *Leishmania* flagellum. Mol. Microbiol. 2008; 70:837–852. [PubMed: 18793337]
71. Vartiainen MK, Mustonen T, Mattila PK, Ojala PJ, Thesleff I, et al. The three mouse actin-depolymerizing factor/cofilins evolved to fulfill cell-type-specific requirements for actin dynamics. Mol. Biol. Cell. 2002; 13:183–194. [PubMed: 11809832]
72. Wetzel DM, Håkansson S, Hu K, Roos D, Sibley LD. Actinfilament polymerization regulates gliding motility by apicomplexan parasites. Mol. Biol. Cell. 2003; 14:396–406. [PubMed: 12589042]
73. Wittekind M, Mueller L. HNCACB, a High-Sensitivity 3D NMR Experiment to Correlate Amide-Proton and Nitrogen Resonances with the Alpha-and Beta-Carbon Resonances in Proteins. J. Magn. Reson. 1993; 101(B):201–205.
74. Yamashiro S, Mohri K, Ono S. The Two *Caenorhabditis elegans* actin depolymerizing factor/cofilin proteins differently enhance actin filament severing and depolymerization. Biochemistry. 2005; 44:14238–14247. [PubMed: 16245940]
75. Yeoh S, Pope B, Mannherz HG, Weeds A. Determining the differences in actin binding by human ADF and cofilin. J. Mol. Bio. 2002; 315:911–925. [PubMed: 11812157]
76. Yonezawa N, Homma Y, Yahara I, Sakai H, Nishida E. A short sequence responsible for both phosphoinositide binding and actin binding activities of cofilin. J. Biol. Chem. 1991; 266:17218–17221. [PubMed: 1654325]
77. Yonezawa N, Nishida E, Iida K, Kumagai H, Yahara I, et al. Inhibition of actin polymerization by a synthetic dodecapeptide patterned on the sequence around the actin-binding site of cofilin. J. Biol. Chem. 1991; 266:10485–10489. [PubMed: 2037594]
78. Yonezawa N, Nishida E, Iida K, Yahara I, Sakai H. Inhibition of the interactions of cofilin, destrin, and deoxyribonuclease-1 with actin by phosphoinositides. J. Biol. Chem. 1990; 265:8382–8386. [PubMed: 2160454]
79. Yonezawa N, Nishida E, Sakai H. pH control of actin polymerization by cofilin. J. Biol. Chem. 1985; 260:14410–14412. [PubMed: 4055781]
80. Zhao H, Hakala M, Lappalainen P. ADF/cofilin binds phosphoinositides in a multivalent manner to act as a PIP 2 -density sensor. Biophysical Journal. 2010; 98:2327–2336. [PubMed: 20483342]

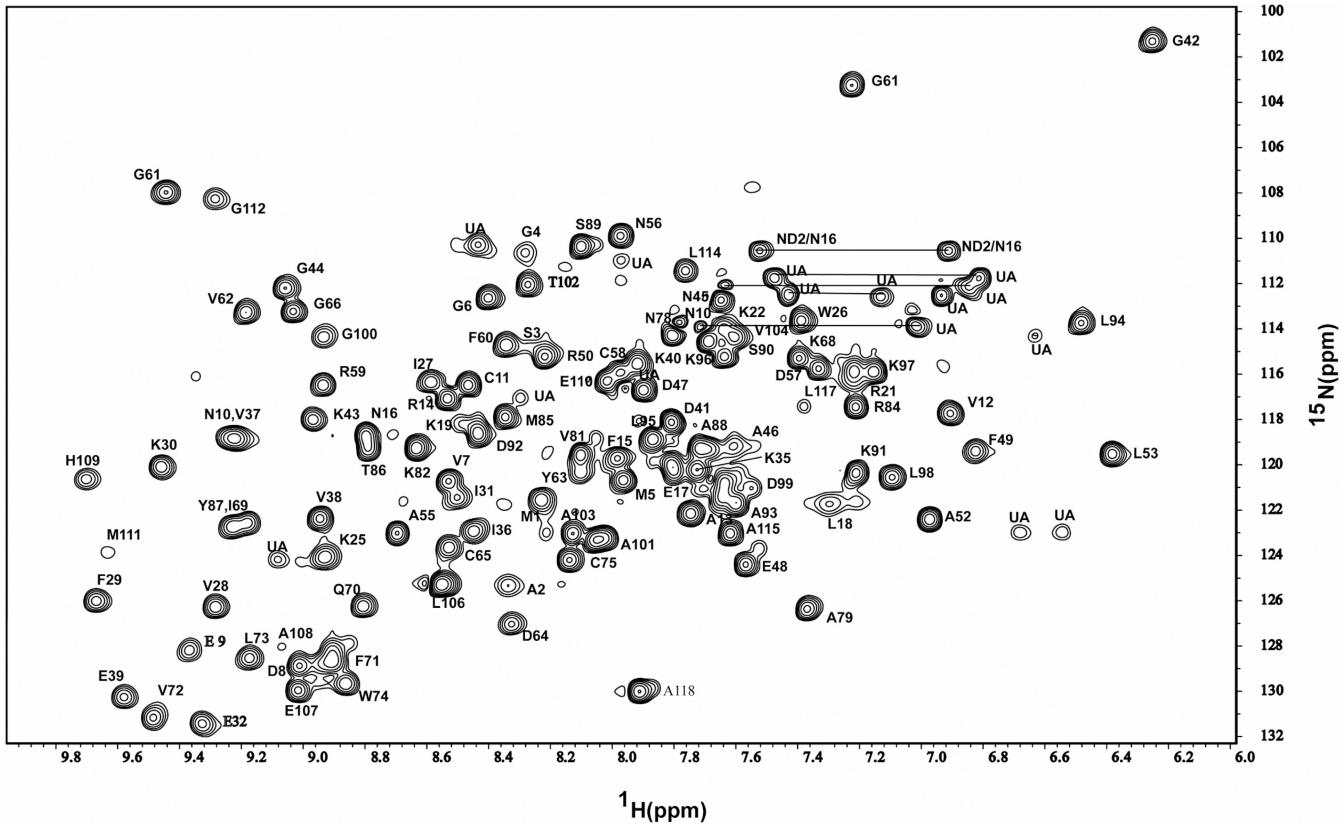

Figure 1.

The ^{15}N-^{1}H HSQC spectrum of 0.8 mM ^{15}N labeled TgADF recorded at 298 K at 600 MHz in 95% H_2O/5% $^{2}H_2O$, 20 mM sodium phosphate buffer, pH 6.5, containing 50 mM NaCl, 0.1% NaN_3, 1 mM DTT, and 1 mM AEBSF. The cross peaks are labeled with single letter amino acid residues name and number in the sequence. Main chain amide proton assignments were not made for the residues Ile20, Thr23, Val24, Asn33, Thr34 and Asn67.

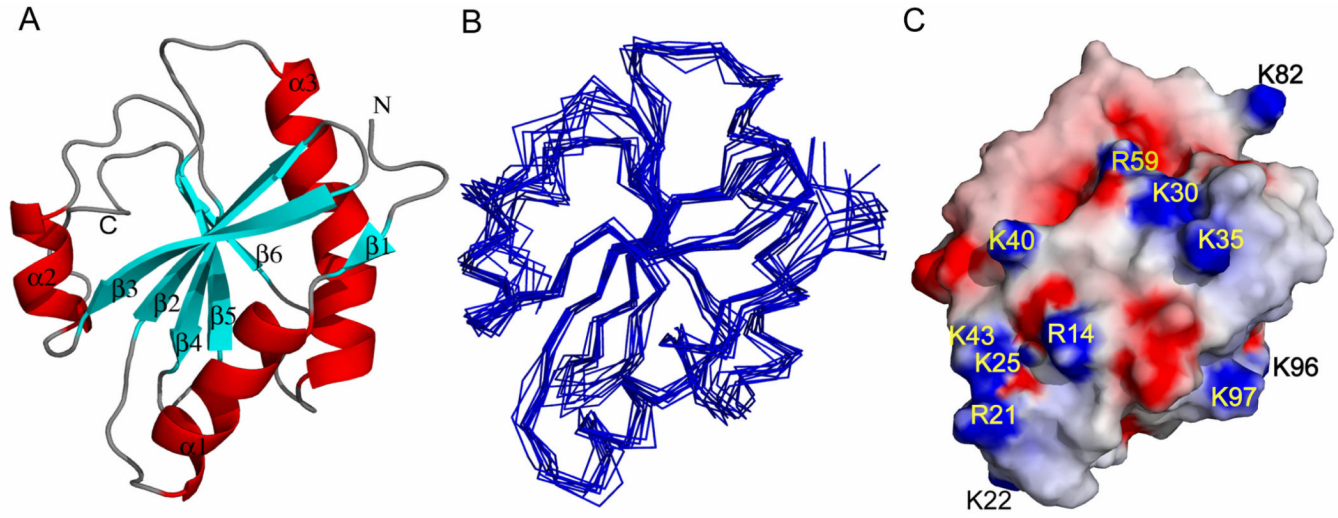

Figure 2.

Solution structure of TgADF. (A) Ribbon diagram of lowest energy structure of TgADF showing six stranded mixed β-sheet surrounded by three α-helices and a C-terminal helical turn. The individual β strands and α helices are labeled. (B) Superimposition of backbone traces from final ensemble of 10 structures with lowest target function. (C) Electrostatic potential of TgADF generated with GRASP. The positively and negatively charged groups are shown in blue and red, respectively.

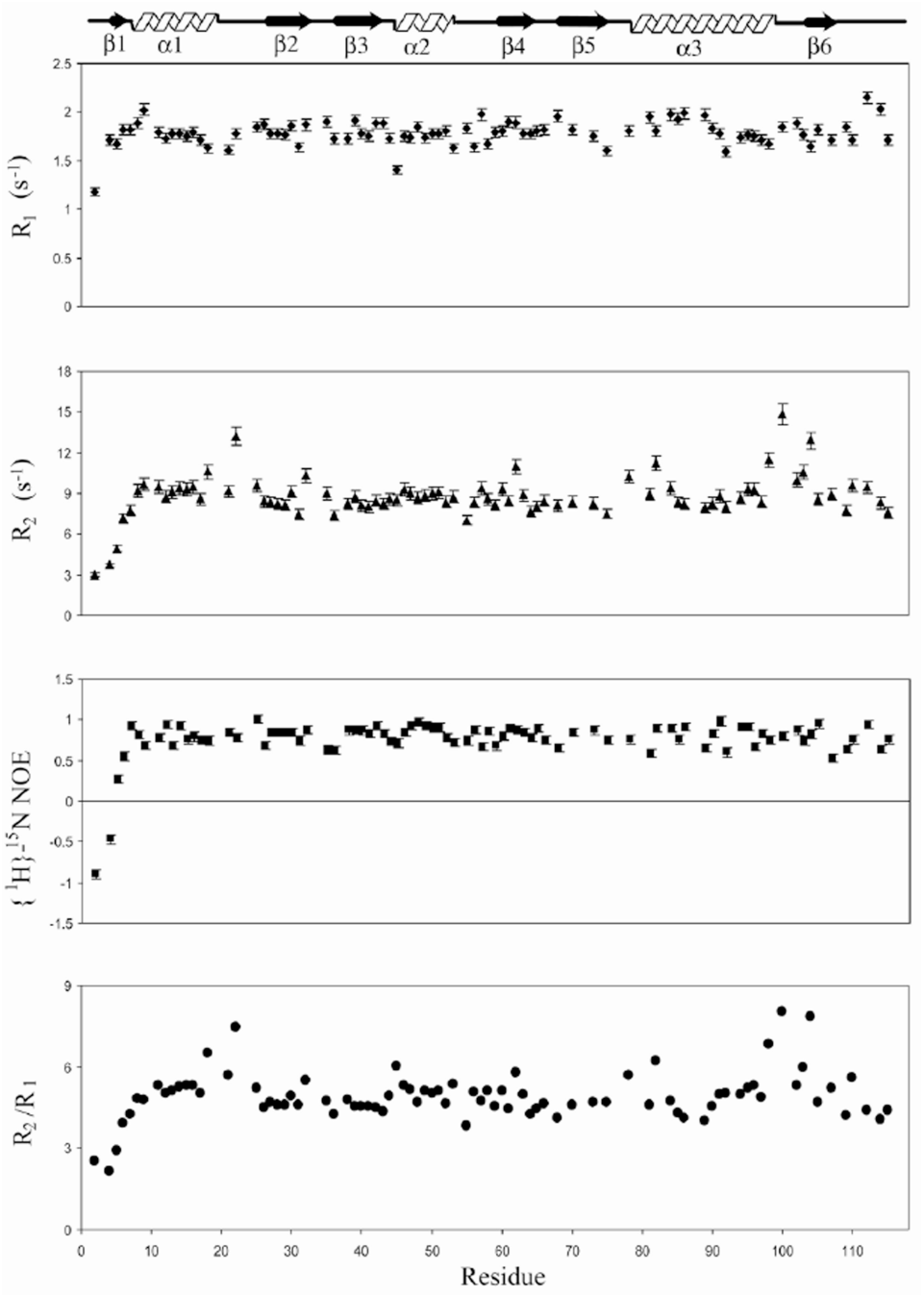

Figure 3.

Sequence dependent variations of backbone ^{15}N relaxation parameters. (a) R_1; (b) R_2; (c) steady state $\{^1H\}$-^{15}N NOE; and (d) R_2/R_1 ratio values of TgADF obtained on 0.8 mM ^{15}N labeled sample at 25 °C on a Varian Inova spectrometer at 600 MHz.

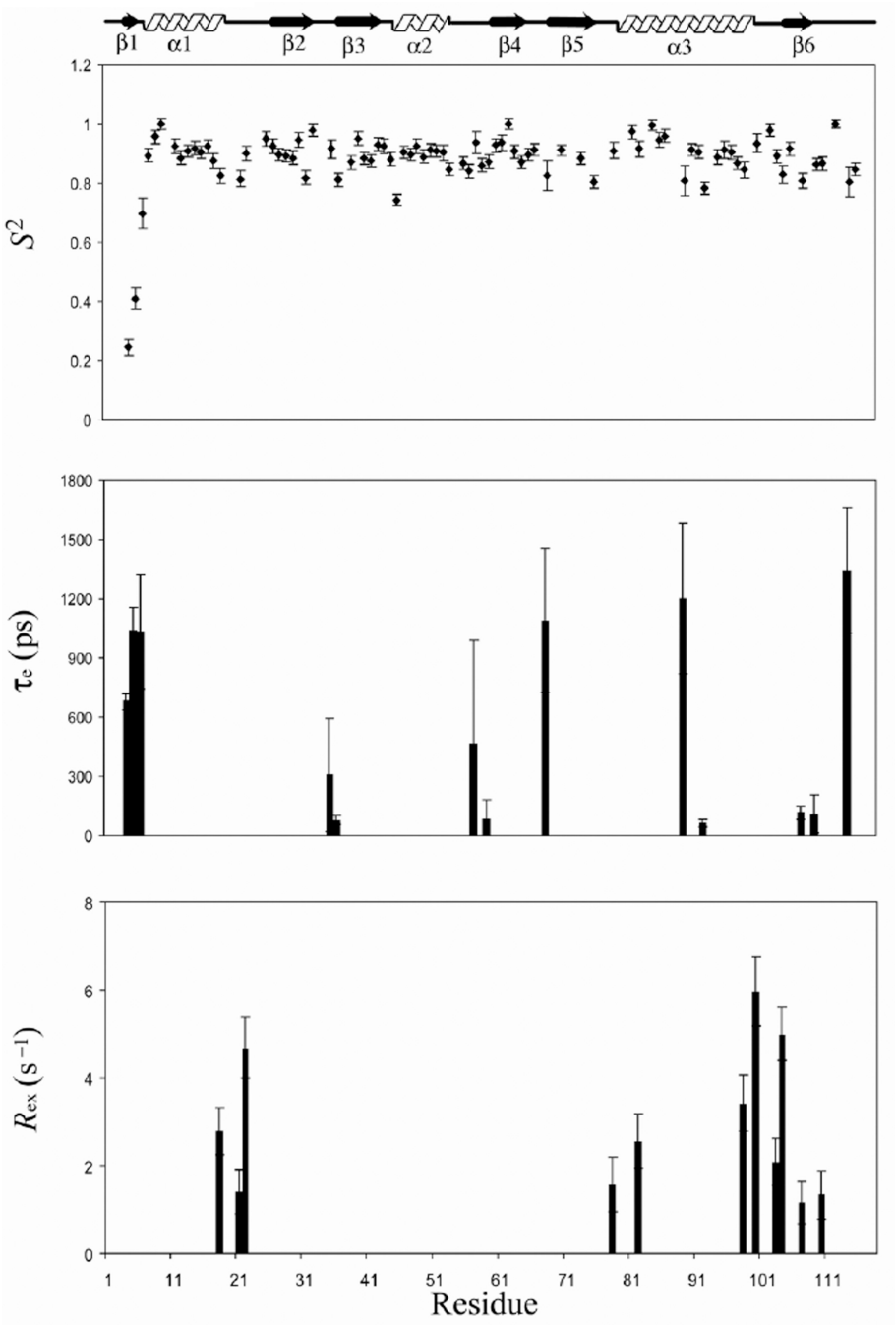

Figure 4.

Plots of optimized Modelfree parameters like generalized order parameter (S^2), the effective correlation time (τ_e) and the chemical exchange parameter (R_{ex}) as a function of residue number for TgADF.

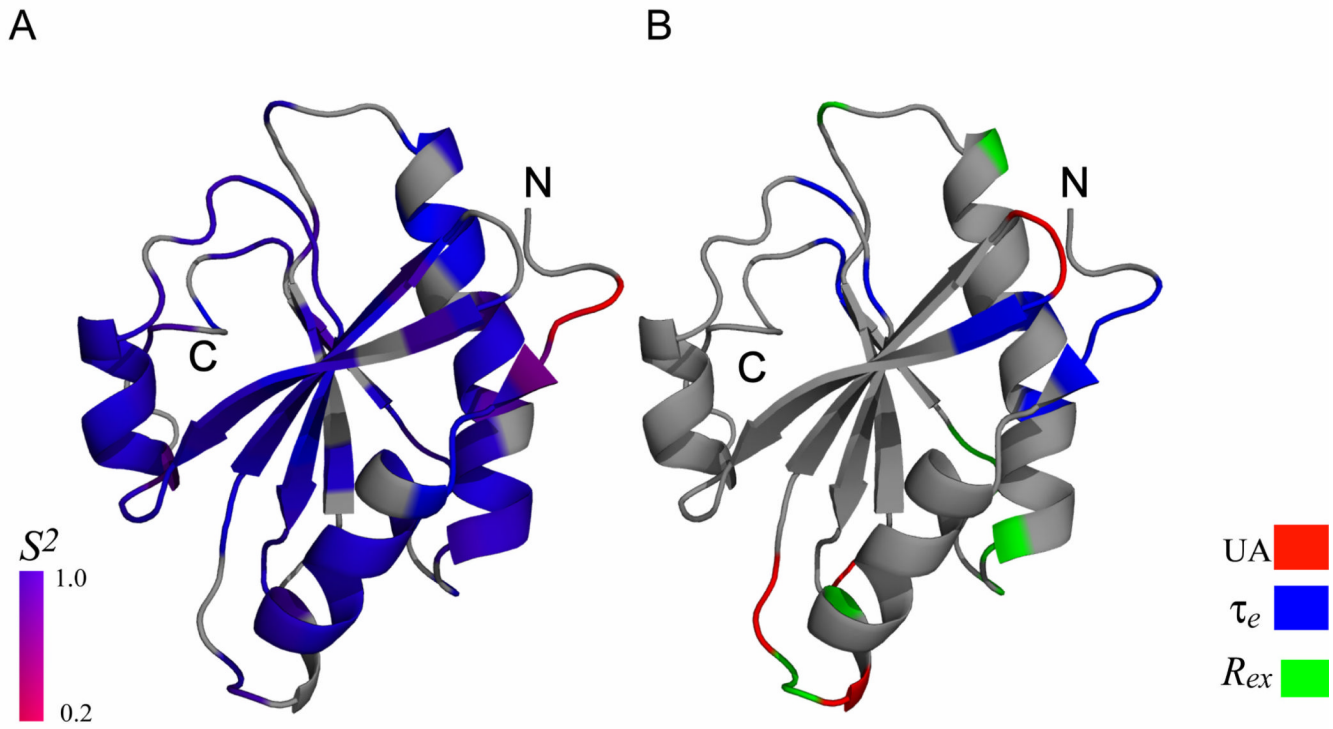

Figure 5.

Backbone dynamics of TgADF from Modelfree analysis. (A) The ribbon representation of TgADF lowest energy solution structure shaded according to the S^2 values derived from Modelfree analysis. The color coding is from blue for S^2=1, to red for S^2=0.2. Prolines and residues that are not included in Modelfree analysis are colored gray. (B) The ribbon representation of TgADF shaded according to chemical exchange (R_{ex}) terms, effective correlation (τ_e) times from Modelfree analysis, and the unassigned residue. The residues displaying conformational exchange are represented in green, while the residues displaying motion on picosecond to nanosecond timescale are represented in blue and the unassigned residues (UA) are colored red.

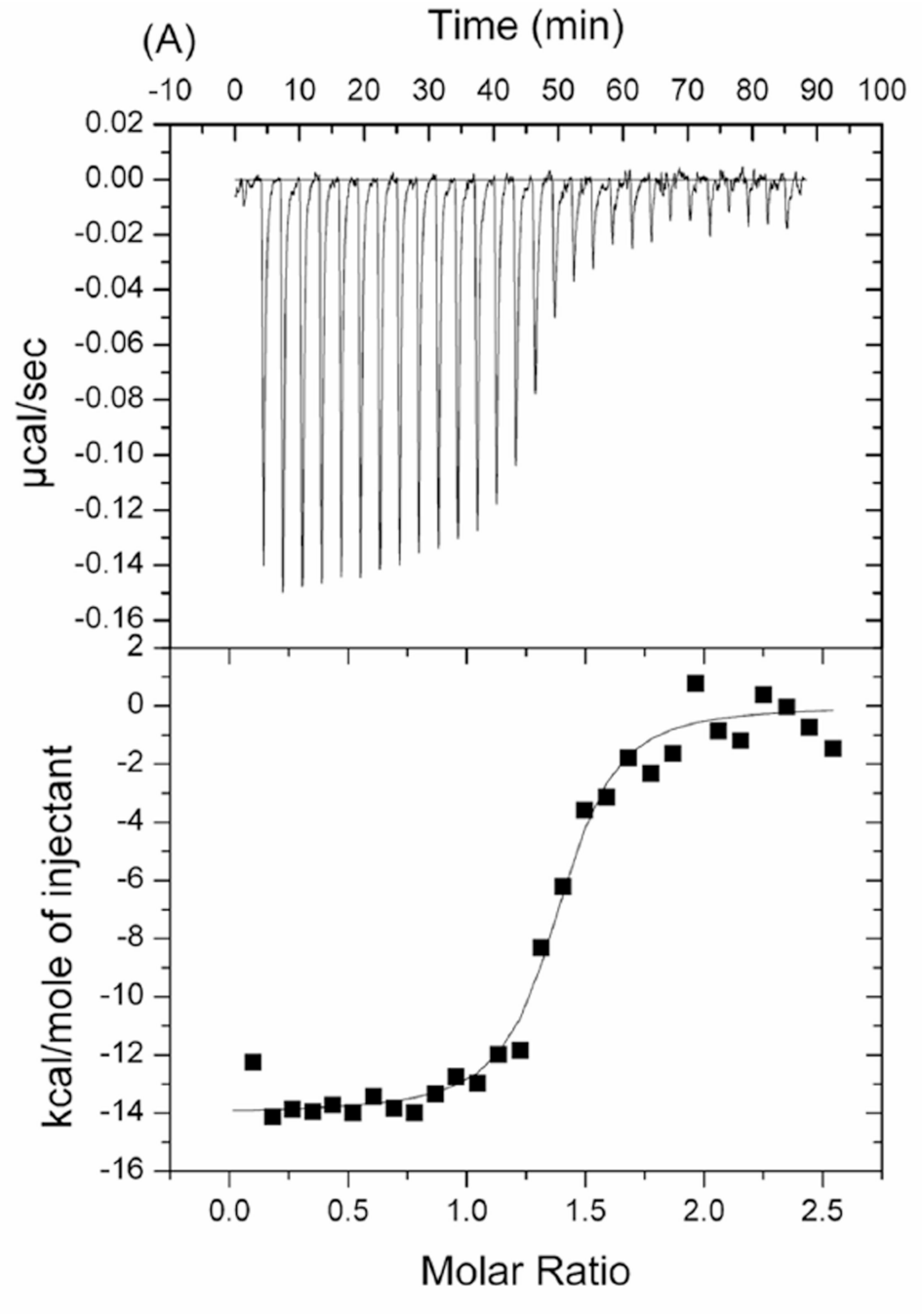

Figure 6.

Probing TgADF-Actin interactions by ITC. The negative peaks indicate an exothermic reaction. The area under each peak represents the heat released after an injection of TgADF into ADP-G-Actin solution. (Lower) Binding isotherms obtained by plotting peak areas against the molar ratio of TgADF to ADP-G-Actin. The lines represent the best-fit curves obtained from least-squares regression analyses assuming a one-site binding model.

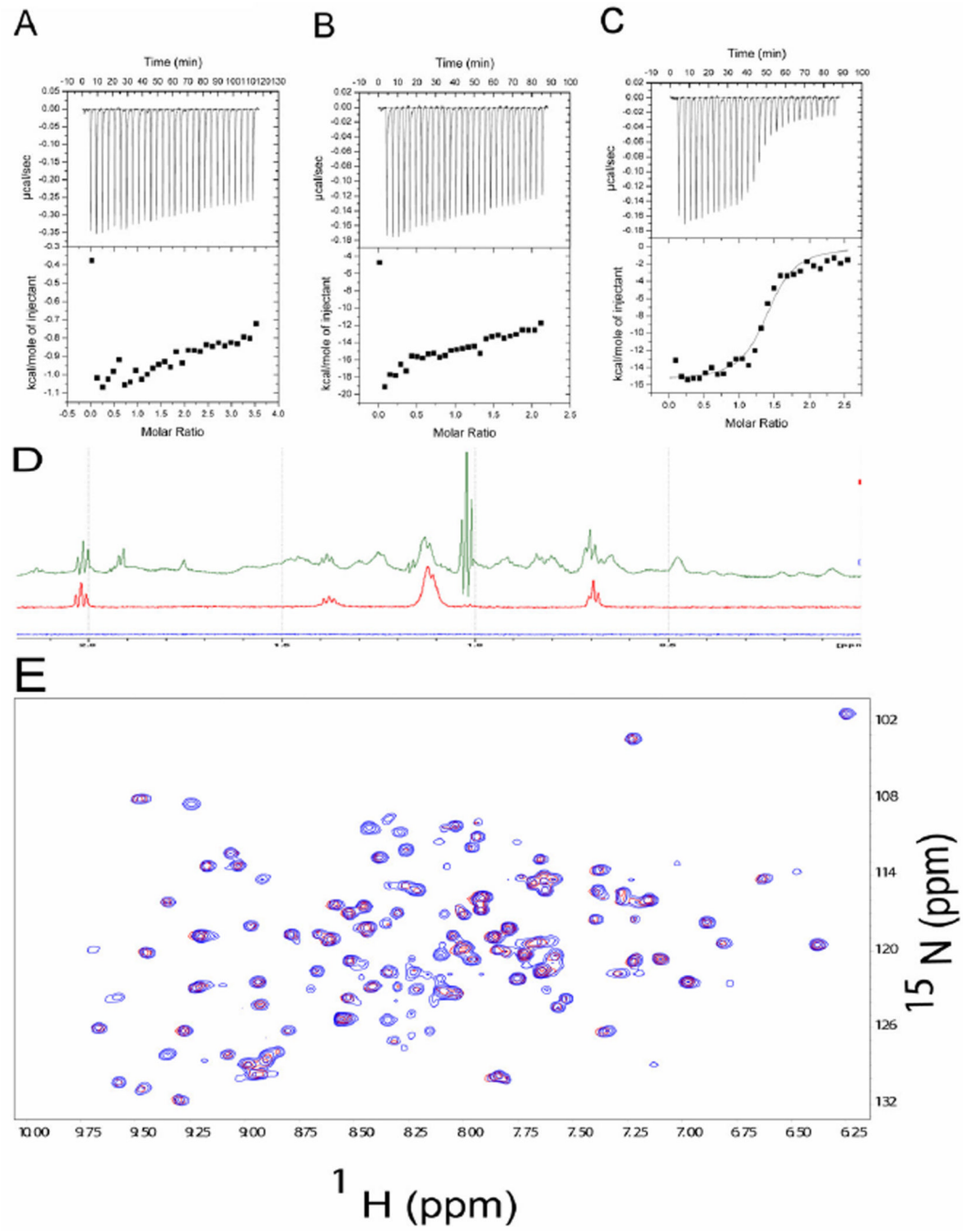

Figure 7.

Probing TgADF - dioctonoyl PI(4,5)P2 interaction by ITC and NMR. The negative peaks indicate an exothermic reaction. The area under each peak represents the heat released after an injection of TgADF into ADP-G-Actin solution. (Lower) Binding isotherms obtained by plotting peak areas against the molar ratio of TgADF to ADP-G-Actin. The lines represent the best-fit curves obtained from least-squares regression analyses assuming a one-site binding model. (A) ITC of TgADF-dioctonoyl PI(4,5)P2. (B) ITC of Rabbit muscle ADP-G-actin-dioctonoyl PI(4,5)P2. (C) TgADF-dioctonoyl PI(4,5)P2+ Rabbit muscle ADP-G-actin. (D) 1-D spectra of buffer (blue), dioctonoyl PI(4,5)P2 (red), dioctonoyl PI(4,5)P2 in

presence of TgADF (green). (E) ^{1}H-^{15}N HSQC spectra overlap of TgADF (red) and TgADF in presence of dioctonoyl PI(4,5)P2 (blue).

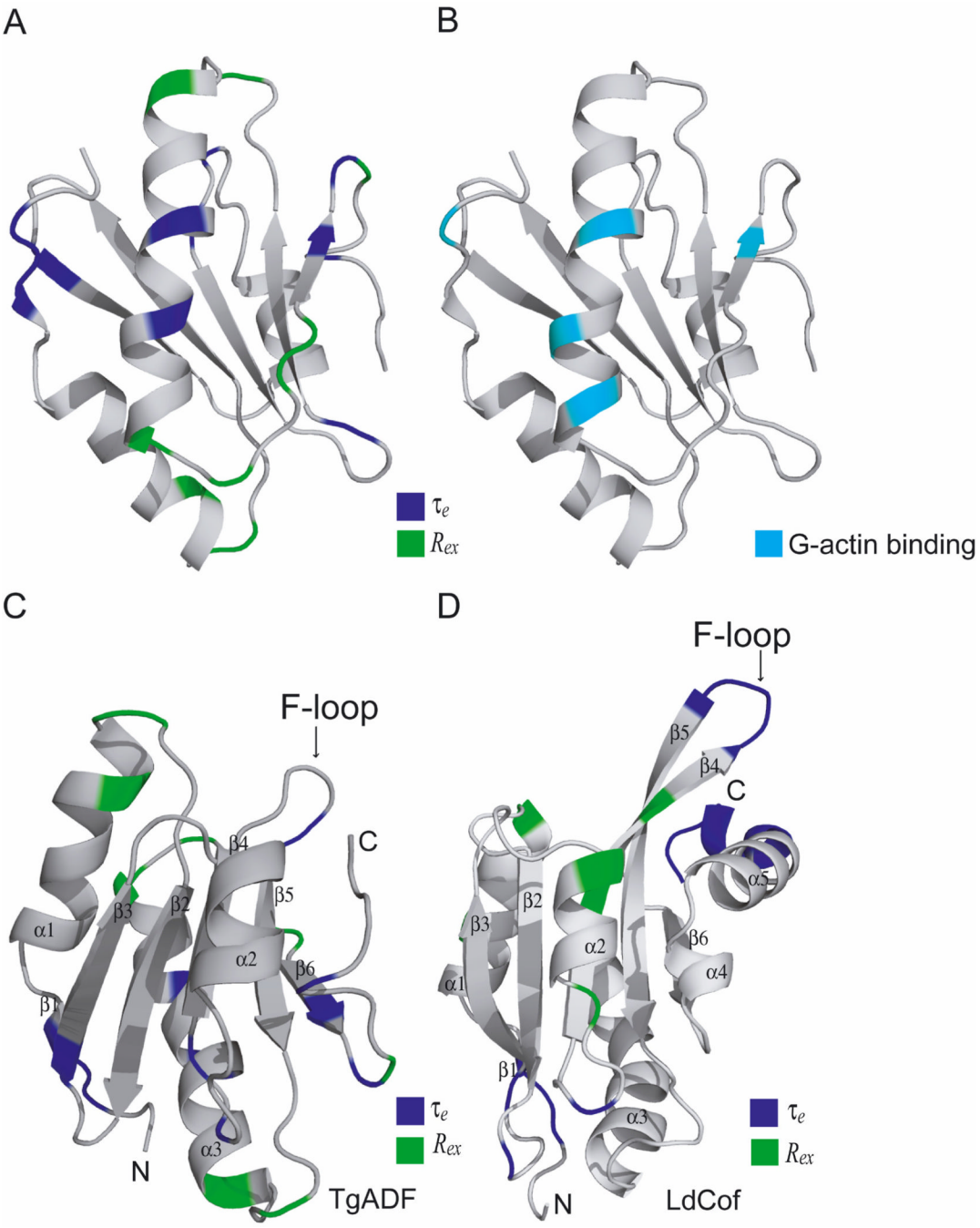

Figure 8.

(A) The ribbon representation of TgADF lowest energy structure shaded according to chemical exchange term (R_{ex}) shaded in green and effective correlation time (τ_e) shaded in blue obtained from model free analysis. (B) Residues involved in hydrogen bonding with G-actin in the TgADF-actin docked model are shaded in cyan. (C) As described for Fig. 8 A with labeled F-loop. (D) The ribbon representation of LdCof lowest energy structure shaded according to chemical exchange term (R_{ex}) and effective correlation time (τ_e) obtained from model free analysis. Color pattern is similar as for TgADF.

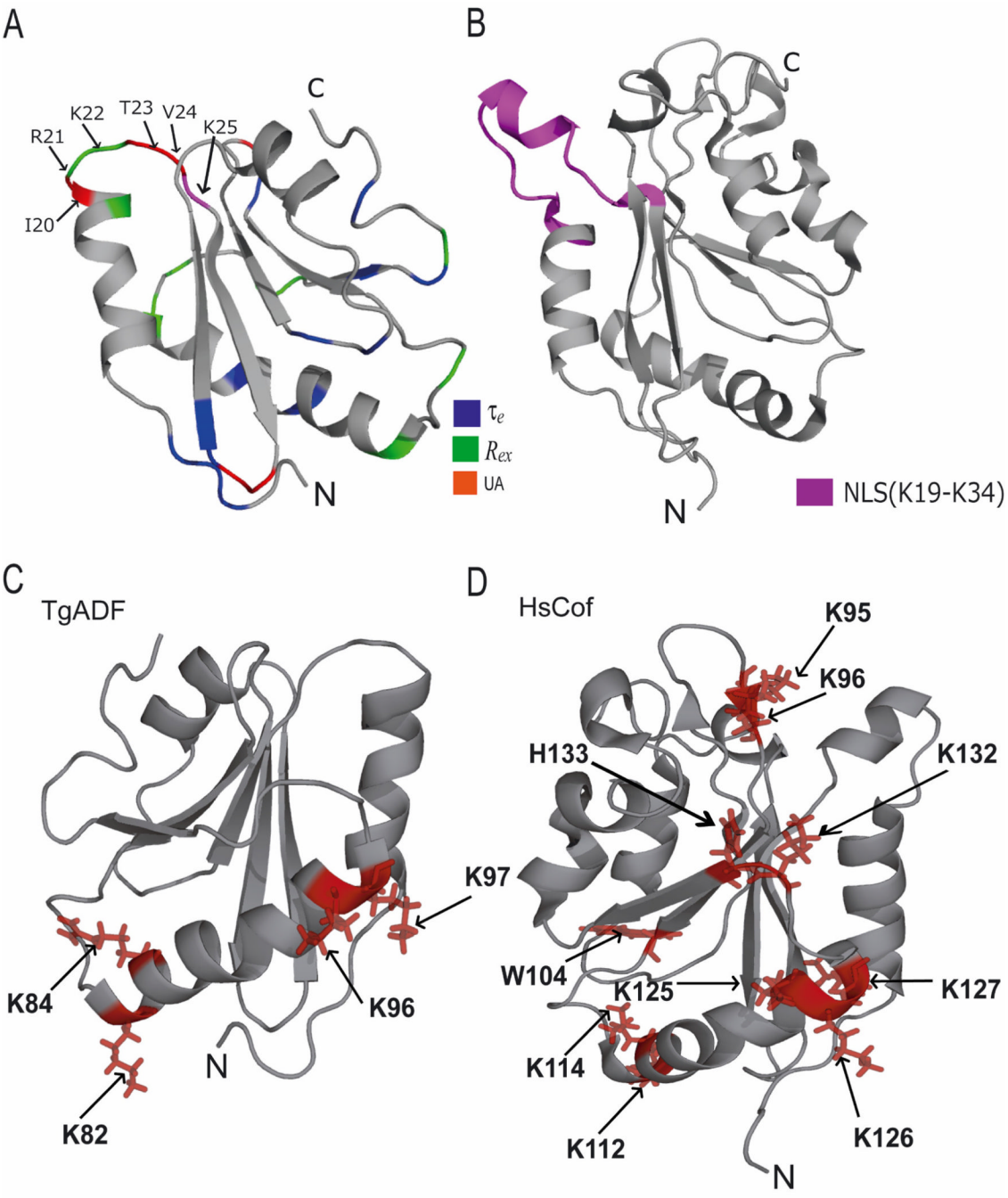

Figure 9.

(A) As described for Fig. 8 A, with the addition of unassigned residues that are colored in red. The region R21-K25 which corresponds with the NLS region of human cofilin-1 (HsCof) has been highlighted and the residue K25 falling in this region is colored in magenta. (B) The ribbon representation of HsCof showing the NLS region (K19–K34) colored in magenta. (C) The ribbon representation of the TgADF lowest energy structure showing the charged residues as stick representations colored in red. These charged residues corresponds to residues important for interaction with dioctanoyl-PI(4,5)P2 in human cofilin-1. (D) The ribbon representation of the HsCof showing residues implicated in interaction with dioctanoyl-PI(4,5)P2 as stick representations colored in red.

Table 1

Experimental restraints and structural statistics for final ensemble of 10 TgADF Structures

Distance Restraint List		
classes	TgADF	
sequential	440	
intra-residual	444	
medium-range	275	
long-range	359	
Hydrogen bonds	47	
Dihedral angle restrains (φ and φ)	192	
RMSD values (Å)	Ordered residues[a] (Å)	
All backbone atoms	0.9	
All heavy atoms	1.3	
Ramachandran plot statistics[a]		
Most favored region (%)	93.3	
Allowed region (%)	6.6	
Additionally allowed region (%)	0.1	
Disallowed region (%)	0.0	
CING ROG analysis[b]		
Red	1	1%
Orange	15	19%
Green	65	80%
WHAT IF Summary[b]		
Structure Z-scores		
1st generation packing quality	−0.527 +/− 1.431	
2nd generation packing quality	5.720 +/− 2.704	
Ramachandran plot appearance	−2.395 +/− 0.385	
chi-1/chi-2 rotamer normality	−3.131 +/− 0.713	
Backbone conformation	0.368 +/− 1.639	
RMS Z-scores		
Bond lengths	1.039 +/− 0.002	
Bond angles	0.290 +/− 0.009	
Omega angle restraints	0.893 +/− 0.097	
Side chain planarity	0.452 +/− 0.085	
Improper dihedral distribution	0.457 +/− 0.018	
Inside/Outside distribution	1.134 +/− 0.032	

[a] region, 2–51, 57–98, 100–108, 112–117

[b] 1–4, 7, 8, 10–13, 15–25, 27, 28, 30, 32, 33, 35–40, 42, 43, 46–50, 53–55, 58–59, 61, 62, 64–67, 69–75, 77–79, 83–89, 93–97, 104–108, 111–113, 118

Table 2

Interface interaction results for docking of crystal structure of actin and TgADF

	ACTIN	TgADF
Number of atom		
Interface	116(4.0%)	89(9.2%)
Surface	1598(55.1%)	582(64.2%)
Total	2901(100%)	906(100%)
Number of residue		
Interface	35(9.4%)	28(23.7%)
Surface	344(92.5%)	115(97.5%)
Total	372(100%)	118(100%)
Solvent accessiblearea,A^2		
Interface	1061(6.2%)	1085.3(16.0%)
Total	17135(100%)	6769.2(100%)
Solvent energy in kcal/mol		
Isolated residue	−378.8(100%)	−103.3(100%)
Gain of complexation	−8.1(2.1%)	−7.2(7.0%)
Average gain	−2.1(0.6%)	−3.0(2.9%)
P-value	0.031	0.0.107

SALT BRIGES Hydrogen Bond			
##	ACTIN	Distance(Å)	TgADF
1	THR 351 (OG1)	3.73	ALA 93 (O)
2	THR 148 (N)	3.27	GLU 107 (OE2)
3	THR 149 (N)	3.72	GLU 107 (OE2)
4	ARG 147 (NE)	3.46	GLU 107 (OE1)
5	GLY 23 (O)	3.80	GLY 4 (N)
6	ALA 144 (O)	3.31	SER 89 (OG)
7	TYR 143 (O)	3.79	SER 89 (N)
8	MET 355 (SD)	2.36	LYS 96 (NZ)

SALT BRIGES			
##	ACTIN	Distance(Å)	TgADF
1	ARG 147 (NE)	3.46	GLU 107 (OE1)